HHS Public Access

Author manuscript

Synapse. Author manuscript; available in PMC 2016 March 01.

Published in final edited form as:

Synapse. 2015 March ; 69(3): 148–165. doi:10.1002/syn.21800.

Female protection from slow-pressor effects of AngII involves prevention of ROS production independent of NMDA receptor trafficking in hypothalamic neurons expressing angiotensin-1A receptors

Jose Marques-Lopes[1], **Mary-Katherine Lynch**[1], **Tracey A. Van Kempen**[1], **Elizabeth M. Waters**[2], **Gang Wang**[1], **Costantino Iadecola**[1], **Virginia M. Pickel**[1,*], and **Teresa A. Milner**[1,2,*]

[1]Brain and Mind Research Institute, Weill Cornell Medical College, 407 East 61st Street, New York, NY 10065

[2]Harold and Margaret Milliken Hatch Laboratory of Neuroendocrinology, The Rockefeller University, 1230 York Avenue, New York, NY 10065

Abstract

Renin-angiotensin system over-activity, up-regulation of post-synaptic NMDA receptor function, and increased reactive oxygen species (ROS) production in the hypothalamic paraventricular nucleus (PVN) are hallmarks of angiotensin II (AngII)-induced hypertension, which is far more common in young males than in young females. We hypothesize that the sex differences in hypertension are related to differential AngII-induced changes in post-synaptic trafficking of the essential NMDA receptor GluN1 subunit and ROS production in PVN cells expressing angiotensin type 1a receptor (AT1aR). We tested this hypothesis using slow-pressor (14 day) infusion of AngII (600ng/kg/min) in mice, which elicits hypertension in males but not in young females. Two month-old male and female transgenic mice expressing enhanced green fluorescent protein (EGFP) in AT1aR-containing cells were used. In males, but not females, AngII increased blood pressure and ROS production in AT1aR-EGFP PVN cells at baseline and following NMDA treatment. Electron microscopy showed that AngII increased cytoplasmic and total GluN1-silver-intensified immunogold (SIG) densities, and induced a trend towards an increase in near plasmalemmal GluN1-SIG density in AT1aR-EGFP dendrites of males and females. Moreover, AngII decreased dendritic area and diameter in males, but increased dendritic area of small (<1μm) dendrites and decreased diameter of large (>1μm) dendrites in females. Fluorescence microscopy revealed that AT1aR and estrogen receptor β do not co-localize suggesting that, if

*Address correspondence to: Drs. Jose Marques Lopes and Teresa A. Milner, Brain and Mind Research Institute, Weill Cornell Medical College, 407 East 61st Street, RM 307, New York, NY 10065, Phone: (646) 962-8274, FAX: (646) 962-0535, joseclopes@gmail.com, tmilner@med.cornell.edu.

*Co-senior authors

CONFLICT OF INTEREST STATEMENT

The authors have no conflict of interest.

ROLE OF AUTHORS

All authors had full access to all the data in the study and take responsibility for the integrity of the data and the accuracy of the data analysis. Study concept and design: JML, EMW, CI and TAM. Preparation of tissue sections: JML, TVK. Acquisition of data: JML, MKL. Analysis and interpretation of data: JML, MKL, TAM. Drafting of the manuscript: JML, TVK, EMW, GW, CI, VMP, TAM. Statistical analysis: JML. Obtained funding: TAM, VMP, CI. Study supervision: TAM.

estrogen is involved, its effect is indirect. The data suggest that the sexual dimorphism in AngII-induced hypertension is associated with sex differences in ROS production in AT1aR-containing PVN cells, but not with post-synaptic NMDA receptor trafficking.

Keywords

paraventricular nucleus; sex differences; angiotensin; blood pressure

INTRODUCTION

The incidence of hypertension is greater in men than in young women, but this condition is reversed at menopause (Martins et al., 2001; Wiinberg et al., 1995). In mice, administration of slow-pressor doses of angiotensin II (AngII) induces hypertension in 2 month-old males, but not in age-matched females (Girouard et al., 2009; Marques-Lopes et al., 2014; Xue et al., 2013a; Xue et al., 2013b). Increasing evidence points to sex differences in central cardiovascular control (Marques-Lopes et al., 2014; Pierce et al., 2009; Wang et al., 2008; Xue et al., 2013a), and differential responses to hypertensive challenges in key brain areas could contribute to sex differences in development and maintenance of hypertension.

AngII plays a pivotal role in human hypertension through diverse mechanisms, and AngII administration is often used as a model of the disease (Biancardi et al., 2014; O'Callaghan et al., 2013; Paton et al., 2008). In the "slow-pressor" model of hypertension, circulating AngII modulates central cardiovascular control via blood-brain barrier-deprived circumventricular organs, e.g., the subfornical organ (SFO) (O'Callaghan et al., 2013). The SFO sends excitatory projections to the hypothalamic paraventricular nucleus (PVN), a key area in central modulation of blood pressure (Ferguson, 2009; Lind et al., 1982; Miselis, 1981). Excitatory SFO input to the PVN leads to local AngII release, and increased expression of angiotensin type 1 (AT1) receptor protein and mRNA (Sriramula et al., 2011; Wei et al., 2009; Wright et al., 1993). Likewise, renin-angiotensin system (RAS) over-activity in the PVN has been shown in spontaneously hypertensive rats (SHR) and in AngII-induced hypertension (Sriramula et al., 2011; Veerasingham and Raizada, 2003; Wei et al., 2009). PVN infusion with AT1 or glutamate receptors blockers decreases blood pressure in hypertensive rats (Freeman and Brooks, 2007; Gabor and Leenen, 2012a; Gabor and Leenen, 2013). In accordance with an interaction between AngII and glutamate, AngII application in hypothalamic slices depolarizes PVN neurons through glutamate release from local interneurons (Latchford and Ferguson, 2004).

Increased glutamatergic transmission in the PVN leads to the sympathoexcitation underlying the hypertension (Ferguson and Latchford, 2000; Gabor and Leenen, 2012b). Up-regulation of post-synaptic NMDA receptor activity in PVN neurons enhances sympathetic outflow in spontaneously hypertensive rats (SHR) and in AngII-induced hypertension (Li and Pan, 2010; Li et al., 2008; Li et al., 2014; Wang et al., 2013; Ye et al., 2012). Augmented reactive oxygen species (ROS) production plays a crucial role in sympathoexcitation associated with AngII-dependent hypertension (Coleman et al., 2013; Jancovski et al., 2013; Wang et al., 2013). Central administration of NADPH oxidase inhibitors attenuates blood pressure

elevation and ROS production in the PVN (Erdos et al., 2006). Prior work from our group has shown increased baseline and NMDA-evoked ROS production in PVN cells, and enhanced association of GluN1 with NADPH oxidase in PVN dendrites of AngII-infused male mice (Wang et al., 2013).

Sex differences in AngII-induced hypertension are associated with greater sympathoexcitation in males than in young females (Xue et al., 2005). We have recently shown that young female mice exhibit protection from AngII-induced hypertension associated with decreased NMDAR density in estrogen receptor (ER) β-containing PVN dendrites (Marques-Lopes et al., 2014). In the PVN, AT1 receptor and ERβ are predominantly expressed in the parvicellular subregion in mouse and rat (Gonzalez et al., 2012; Hauser et al., 1998; Laflamme et al., 1998; Lenkei et al., 1997; Milner et al., 2010), and co-localize with corticotropin-releasing factor (CRF) in rat (Aguilera et al., 1995; Laflamme et al., 1998). Thus, neurons containing AT1a receptor might co-localize ERβ and be susceptible to local estrogen-mediated modulation of neuronal activity. Therefore, the present study sought to determine whether AngII infusion leads to differential changes in baseline and NMDA-evoked ROS production and in post-synaptic GluN1 density and trafficking in AT1aR-expressing cells of the PVN in male and female mice. In addition, immunohistochemical analysis was performed to assess AT1 receptor and ERβ co-localization in the PVN. Finally, retrograde tracing was used to evaluate if mouse PVN AT1aR-containing neurons project to the median eminence (Hashimoto et al., 2004) and/or to the presympathetic neurons of the intermediolateral cell column (IML) of the spinal cord (Nunn et al., 2011).

MATERIALS AND METHODS

Animals

General—Experimental procedures were approved by the Institutional Animal Care and Use Committees of Weill Cornell Medical College and were in accordance with the 2011 Eighth Edition of the National Institute of Health Guide for the Care and Use of Laboratory Animals. Studies were conducted in Agtr1a bacterial artificial chromosome (BAC) transgenic mice that express AT1aR identified by enhanced green fluorescent protein (AT1aR–EGFP) (Gonzalez et al., 2012). Details on the characterization of this mouse have been described previously (Gonzalez et al., 2012). Briefly, AT1aR-EGFP mice were originally developed by the GENSAT project (www.gensat.org) at The Rockefeller University (Gong et al., 2003). Hemizygote BAC-based AT1aR transgenic mice were originally on a FVB/N background and were back-crossed with C57BL/6 mice for six generations. Males and females between 2–3 months-old at the beginning of the experiment were used. Mice were housed 3–4 animals per cage with 12:12 light/dark cycles with *ad libitum* access to food and water. All survival surgeries were done using isofluorane anesthesia (induction 5%; maintenance 1.5–2% in oxygen),

Estrous cycle determination—Estrous cycle stage was determined using vaginal smear cytology (Turner and Bagnara, 1971) daily between 9:00 and 10:00 AM. In young (pre-menopausal) mice, estrous cycles last 4–5 days and consist of 3 primary phases: proestrus

(high estrogen levels; 0.5–1 day), estrus (declining estrogen levels; 2–2.5 days) and diestrus (low estrogen and progesterone levels; 2–2.5 days). Previous studies have shown variability in AT1 receptor density across the estrous cycle in the pituitary (Seltzer et al., 1992) and in the dorsomedial arcuate nucleus (Seltzer et al., 1993). Therefore, estrous cycle determination was performed to ensure that only females with two regular estrous cycles prior to beginning the experiment were used. No females in proestrus at day 14 after mini-pumps implantation were included in the analyses. To control for effects of handling, male mice were removed from their cage and handled daily.

Retrograde labeling of spinally projecting PVN neurons—Male mice (N=3) were anesthetized as above and their spinal cords were exposed at the T2–T4 level through dorsal laminectomy. Using a custom-made Hamilton syringe (Model 75 SN SYR, 5 μl, 32 gauge; Reno, NV), 1 μl of 4% Fluorogold (FG, Fluorochrome Inc., Denver, CO) was pressure injected into the IML region of the spinal cord and the incision was sutured after the injection (Li et al., 2008; Marques-Lopes et al., 2014; Wang et al., 2013). Mice were euthanized 9 days after surgeries. Injection site was verified in spinal cord sections encompassing the T2–T4 region. Successful injections were centered in the IML. Limited lateral diffusion of FG into the intermediomedial nucleus was observed.

Labeling of neuroendocrine PVN neurons—Male mice (N=3) were anesthetized as above and injected with 50 μl of 1% fluorogold (FG; Fluorochrome, Denver, CO) into the tail vein using a 27G ½ insulin syringe (BD Biosciences, San Diego, CA), as described previously (Biag et al., 2012). Mice were euthanized 7 days after injections.

Slow pressor AngII administration—Mice were anesthetized as above and osmotic mini-pumps (Alzet, Durect Corporation, Cupertino, CA) containing vehicle (saline+0.01% bovine serum albumin – BSA) or AngII (600 ng · kg–1 · min–1) were implanted subcutaneously in males and females (N=8–10 mice/group). Systolic blood pressure (SBP) was measured in awake mice by tail-cuff plethysmography (Model MC4000; Hatteras Instruments, Cary, NC), as described previously (Coleman et al., 2010) prior to (baseline), and 2, 5, 9 and 13 days after mini-pump implantation. The limitations of using tail-cuff plethysmography to measure SBP have been discussed previously (Marques-Lopes et al., 2014). To minimize stress, the animals were handled by the same experimenter and at the same time of day throughout the study. Mice were euthanized one day after the final SBP measurements (Coleman et al., 2013; Marques-Lopes et al., 2014; Wang et al., 2013).

ROS detection—ROS production was determined using dihydroethidium (DHE). Superoxide oxidizes the cell-permeant DHE to 2-hydroxyethidium and other oxidation products (Zhao et al., 2005; Zhao et al., 2003), which interact with DNA and are detectable by fluorescence microscopy. ROS production was measured in dissociated PVN cells from male and female mice after 14 d of vehicle or AngII infusion (n = 13–16 cells/group, from 5–7 mice each). Dissociation of PVN cells was performed with 90 min incubation as described previously (Coleman et al., 2013) with 0.02% pronase and thermolysin (Sigma-Aldrich, St Louis, MO) in Mg^{2+}-free lactic acid-artificial cerebrospinal fluid. Identification of cells and ROS detection were performed as described previously (Girouard et al., 2009;

Wang et al., 2013). Bath application of 100 μM NMDA was performed after a stable baseline measurement was achieved. NMDA is known to induce NOX2-dependent free radical production in the brain (Girouard et al., 2009). The increase in ROS signal induced by NMDA was expressed as the ratio of Ft/Fo, where Ft is fluorescence after application of NMDA, and Fo is the baseline fluorescence in the same cell (Girouard et al., 2009; Wang et al., 2006; Wang et al., 2013).

Immunocytochemical procedures

Antisera—For labeling of EGFP, a chicken polyclonal anti-GFP antibody (GFP-1020; Aves Lab Inc., San Diego, CA) was used. The GFP antibody was generated against recombinant GFP and recognizes the gene product of EGFP-expressing transgenic mice (Encinas et al., 2006). The specificity of this antibody has been demonstrated by immunohistochemistry and Western blot using GFP-expressing transgenic mice, resulting in one major band at ~27 kD (see data sheet for EGFP-1020 at www.aveslab.com). Moreover, absence of labeling has been shown in brain sections from mice that lack EGFP (Milner et al., 2011; Volkmann et al., 2010). Previously, we showed that the distribution of AT1aR-EGFP cells in the brain closely corresponds to that obtained with labeling of AngII and AT1 receptor protein and mRNA (Gonzalez et al., 2012).

For labeling of GluN1, a monoclonal mouse anti-GluN1 antibody (clone 54.1; BD Biosciences) was used. Western blot analysis of a lysate from rat cortex probed with the anti-GluN1 antibody resulted in one major band at ~120 kD. HEK 293 cells transfected with cDNA encoding GluN1 displayed similar results whereas non-transfected cells resulted in no bands (see data sheet for anti-NMDAR1 at www.biosciences.com). Injection of rAAV-cre into the nucleus accumbens of floxed GluN1 mice leads to a 40% reduction of GluN1-immunoreactivity (Beckerman and Glass, 2012; Glass et al., 2013).

To label ERβ, an anti-ERβ antibody raised in rabbits (Z8P; Zymed Laboratories, San Francisco, CA) was used. This antibody recognizes a peptide sequence in the C-terminus (aa 468–485) of the mouse ERβ protein (Shughrue and Merchenthaler, 2001). Specificity for ERβ has been shown by Western blot, double label with mRNA using in situ hybridization, preadsorption control and absence of labeling in fixed brain sections prepared from ERβ knockout mice (Creutz and Kritzer, 2002; Shughrue and Merchenthaler, 2001).

To label FG, an anti-FG antibody raised in guinea pig (Protos Biotech Corp, New York, NY) was used. We and others have shown selective staining of retrogradely labeled neurons using this antiserum in mouse PVN (Marques-Lopes et al., 2014), mouse hippocampus (Jinno and Kosaka, 2002), rat PVN (Perello and Raingo, 2013), and rat spinal cord (Polgar et al., 2007). Immunostaining is completely blocked by preincubation with FG or Fast Blue (see data sheet for NM-101 at www.protosantibody.com).

For labeling of arginine-vasopressin (AVP), a polyclonal anti-AVP antibody raised in guinea pig (Peninsula Laboratories Inc., San Carlos, CA) was used. Immunostaining is completely abolished by preadsorption (Hundahl et al., 2010). Moreover, no staining is observed in the Brattleboro rat, which is unable to produce AVP due to a natural genetic mutation (Drouyer et al., 2010).

Tissue preparation

Fluorescence microscopy: Spinally and tail vein-injected mice (described above) and additional female AT1aR-EGFP mice (N = 5) were used to study if AT1aR and ERβ co-localize in the PVN. Mice were deeply anesthetized with sodium pentobarbital (150 mg/kg, i.p.) and their brains fixed by aortic arch perfusion sequentially with 2–3 ml saline (0.9%) containing 2% heparin followed by 30 ml of 4% paraformaldehyde (PFA) in 0.1M sodium phosphate buffer (PB; pH 7.4). After the perfusion, the brains were post-fixed for 24 h in PFA at 4°C.

Immunoelectron microscopy: Three animals per group (males/females infused with AngII/saline) were deeply anesthetized with sodium pentobarbital as above and fixed by aortic arch perfusion sequentially with 2–3 ml saline (0.9%) containing 2% heparin followed by 30 ml of 3.75% acrolein and 2% PFA in PB (Milner et al., 2011). After the perfusion, brains were removed and post-fixed for 30 min in 2% acrolein and 2% PFA in PB at room temperature. Brains were then cut into 5 mm coronal blocks using a brain mold (Activational Systems, Inc., Warren, MI) and sectioned (40 μm thick) on a VT1000X Vibratome (Leica Microsystems, Buffalo Grove, IL). Brain sections were stored at −20°C in cryoprotectant until immunohistochemical processing (Milner et al., 2011).

To ensure identical labeling conditions between experimental groups for quantitative studies (Pierce et al., 1999), two sections per animal encompassing the region of the PVN [0.70–0.94 mm caudal to bregma; Fig. 1A (Hof et al., 2000)] were marked with identifying punches, pooled into single containers and then processed through all immunohistochemical procedures together.

Dual labeling Immunofluorescence—One in every three PVN sections was removed from the cryoprotectant, rinsed thoroughly in PB and incubated in 1% BSA in PB for 2 h to minimize nonspecific binding of the antisera. Sections were incubated with combinations of appropriate primary antisera to **1)** GFP (1:10,000) and ERβ (1:1000), **2)** EGFP and FG (1:2000), **3)** and GFP, AVP (1:1200) and FG. Primary antisera were incubated in PB with 0.5% bovine serum albumin (BSA) and 0.1% Triton X-100. **1)** Incubation in anti-ERβ antibody was done at room temperature. At 24 h, the tissue was moved to 4°C. Anti-GFP antiserum was added to the primary antibody diluent at 96 h time-point and the tissue incubated for additional 24 h; **2)** Incubation in anti-GFP and anti-FG antisera was done at room temperature for 24 h; **3)** Incubation in anti-GFP, anti-AVP and anti-FG antisera was done at room temperature. At 24 h, the sections were moved to 4°C for additional 24 h. Sections were rinsed in PB and incubated for 2h with combinations of appropriate secondary antibodies conjugated with Alexa Fluor dyes (1:400 dilution; Invitrogen-Molecular Probes, Carlsbad, CA). Alexa Fluor 488 goat anti-chicken IgG and Alexa Fluor 647 goat anti-rabbit pig IgG Sections were mounted on gelatin-coated slides, air-dried and coverslipped with slowFade Gold reagent (Invitrogen-Molecular Probes, Grand Island, NY).

Dual label electron microscopic immunocytochemistry—Tissue sections were processed using a pre-embedding dual immunolabeling protocol, as described previously (Milner et al., 2011). The tissue was treated with 1% sodium borohydride in PB for 30 min

to neutralize reactive aldehydes and rinsed thoroughly in PB. Free-floating sections were immersed in 0.5% bovine serum albumin (BSA) in 0.1 M tris saline, pH 7.6 (TS) for 30 min. The tissue then was incubated at room temperature in a solution of anti-GluN1 (1:50) antiserum in TS with 0.01% BSA for 48 h. Anti-GFP (1:2500) antiserum was added to the primary antibody diluent at 24 h and the tissue was moved to 4°C.

For immunoperoxidase detection of GFP, sections were placed for 30 min in goat anti-chicken IgG (1:400; Jackson ImmunoResearch Inc., West Grove, PA), followed by 30 min incubation in avidin–biotin complex (Vector Laboratories, Burlingame, CA). After rinsing in TS, the bound peroxidase was visualized by reaction of the sections for 6–7 min in 3,3′-diaminobenzidine (DAB; Sigma-Aldrich Chemical Co., Milwaukee, MI) and hydrogen peroxide.

For immunogold detection of GluN1, the DAB-reacted sections were rinsed and placed overnight in a 1:50 dilution of donkey anti-goat IgG with bound 1 nm colloidal gold [Electron Microscopy Sciences (EMS), Fort Washington, PA]. The gold particles were fixed to the tissue in 2% glutaraldehyde in 0.01M phosphate-buffered saline (PBS, pH 7.4) and rinsed in PBS followed by 0.2 M sodium citrate buffer (pH 7.4). Bound silver–gold particles were enhanced using a Silver IntenSE M kit (RPN491; GE Healthcare, Waukeska, WI) for 7 min.

Tissue sections were postfixed in 2% osmium tetroxide for 1 hr, dehydrated through a series of graded ethanols and propylene oxide, and flat-embedded in Embed-812 (EMS) between two sheets of Aclar plastic. Ultrathin sections (70 nm thickness) from the PVN were cut with a diamond knife (EMS) using a Leica EM UC6 ultratome. The sections were collected on 400-mesh thin-bar copper grids (EMS) and counterstained with uranyl acetate and lead citrate.

Light microscopic analysis—Sections containing the PVN (Fig. 1A) labeled for AT1aR-EGFP using immunoperoxidase were photographed with a Nikon 80i light microscope equipped with Micropublisher a digital camera (Q-imaging, Barnaby, British Columbia, Canada).

Immunofluorescence microscopic analysis—Photographs of spinal tract-tracing, ERβ+AT1aR-EGFP labeling and neuroendocrine PVN neurons were acquired using a Leica (Nussloch, Germany) confocal microscope. Z-stack analysis was employed to verify dually labeled neurons. Sections from spinal tract-tracing and ERβ+AT1aR-EGFP reactions were collected from three different rostrocaudal levels encompassing the PVN [approx. −1.1, −1.6, −2.1 mm from Bregma (Hof et al., 2000)].

Ultrastructural data analyses—Sections were examined using a Tecnai transmission electron microscope. Images were collected at a magnification of 13,500. Profiles containing GluN1 with GFP immunoreactivity were classified as neuronal (soma, dendrites, axons, terminals) or glial based on criteria described by Peters et al. (1991). Dendritic profiles contained regular microtubular arrays and were usually postsynaptic to axon terminal profiles.

An equal amount of tissue from each treatment group (9596 μm^2/group) was sampled for electron microscopic analysis. Immunoperoxidase labeling for GFP was distinguished as an electron-dense reaction product precipitate. Silver-intensified immunogold (SIG) labeling for GluN1 appeared as black electron-dense particles. Criteria for field selection, and measures to avoid false-negative labeling of smaller profiles, variability between animals in each experimental group and differential reagent sensitivity comparing SIG and immunoperoxidase labeling were performed as described before (Milner et al., 2011; Pierce et al., 1999) Tissue collection from each block was terminated when 50 images of dual labeled dendritic profiles were taken. Analysis of GluN1-SIG density in non-AT1aR-containing dendrites was not performed, as these dendrites arise from a mixed population of neurons.

The subcellular distribution and density of GluN1-SIG particles in AT1aR-EGFP-labeled dendrites was determined as previously described (Coleman et al., 2013). For this, GluN1-SIG particle localization was categorized as (1) plasmalemmal, (2) near plasmalemmal (particles not touching but within 70 nm from the plasma membrane), or (3) cytoplasmic. The investigator performing the quantification of SIG particles was blinded to sex and experimental condition. Microcomputer Imaging Device software (MCID, Imaging Research Inc, Ontario, Canada) was used to determine cross-sectional diameter, perimeter, surface area, form factor, and major and minor axis lengths of each immunolabeled dendrite. Dendrites with an oblong or irregular shape (form factor value < 0.5) were excluded from the dataset. The parameters used for statistical comparisons were as follows: (1) number of plasmalemmal GluN1-SIG particles on a dendrite/dendritic perimeter, (2) number of near plasmalemmal GluN1-SIG particles, (3) number of cytoplasmic GluN1-SIG particles/ dendritic cross-sectional area, and (4) total GluN1-SIG particles (sum of plasmalemmal, near plasmalemmal *and* cytoplasmic) in a dendritic profile. Dendrites were further divided in small (> 1.0 μm) and large (< 1.0 μm) based on average diameter, which correspond with distal and proximal to the cell body (Peters et al., 1991). Moreover, comparisons of GluN1-SIG counts, and dendritic area and average diameter were performed across all groups.

Statistical analysis

Two-way ANOVAs with sex (male, female) and condition (AngII, saline) as between-subjects factors were used to analyze SBP, and SIG density and counts. Repeated measures ANOVA with sex (male, female) and condition (AngII, saline) as between-subjects factors, and NMDA administration (baseline, NMDA) as within-subjects factor was used to compare ROS production. Bonferroni post-hoc test was subsequently used. Data are expressed as means ± SEM. Values were considered statistically significant when $p < .05$.

Figure preparation

Images were cropped in Adobe Photoshop 9.0 or PowerPoint 2010. Final adjustments to brightness, contrast, sharpness and size were done in PowerPoint 2010. These changes did not alter the original content of the raw image. Graphs were generated in Prism 5 (GraphPad Software, La Jolla, CA).

RESULTS

Distribution of AT1aR-EGFP-labeled cells in the PVN

As described previously (Gonzalez et al., 2012), low magnification showed dense packing of AT1aR-EGFP-labeled cells in the PVN (Fig. 1B). At higher magnification, thick, straight, dendritic-like processes of AT1aR-EGFP neurons could be distinguished (Fig. 1B, Inset).

By electron microscopy, GluN1-SIG were localized in the cytoplasm, near the plasmalemma, and on the plasma membrane of AT1aR-EGFP-containing dendrites (examples in Fig. 1C). GluN1-SIG particles also were observed in AT1aR-EGFP-labeled terminals, somata and glial profiles, and in non-AT1aR-containing dendrites, terminals and glia (not shown). AT1aR-EGFP-containing dendrites were contacted by numerous terminals, some of which formed asymmetric (excitatory-type) synapses.

Characterization and projections of AT1aR-EGFP cells in the PVN

In agreement with previous studies (Gonzalez et al., 2012; Hauser et al., 1998; Laflamme et al., 1998; Lenkei et al., 1997; Milner et al., 2010), immunofluorescence microscopy showed dense packing of both AT1aR-EGFP and ERβ-containing cells in the PVN, predominantly in the parvicellular subnucleus (Fig. 2A–C). The number of AT1aR-EGFP- and ERβ-containing cells was similar across the three rostrocaudal PVN levels analyzed. A total of 1507 AT1aR-EGFP- and 574 ERβ-labeled cells were counted in the PVN. Only 3 double-labeled cells were detected, showing that AT1aR and ERβ are contained in different neuronal populations in the mouse PVN.

Spinally projecting PVN neurons are critically involved in the increased sympathetic activity observed in hypertension (Nunn et al., 2011). FG-labeled neurons were found bilaterally and mostly overlapping with AT1aR-EGFP in the parvicellular subnucleus of the PVN (Fig. 2D–F). Approx. 81% of FG-labeled neurons were observed at −1.6 mm from Bregma (Hof et al. 2000). A total of 1005 AT1aR-EGFP- and 379 FG-containing cells were counted. No double-labeled cells were detected, showing that mouse PVN AT1aR-expressing neurons do not project to the spinal cord.

In agreement with our previous study (Gonzalez et al., 2012), AT1aR-EGFP cells were intermixed but not co-localized with AVP, a marker of magnocellular neurons (Coleman et al., 2009), suggesting that most AT1aR-EGFP cells are parvicellular (Fig. 2G,H).

FG injected into the bloodstream labels PVN neurons that project to the median eminence and posterior pituitary, which are devoid of blood-brain barrier (Swanson and Kuypers, 1980; Swanson and Sawchenko, 1980). Scarce co-localization of AT1aR-EGFP and tail vein-injected FG was found in PVN neurons, suggesting that most AT1aR-EGFP neurons are not directly involved in neuroendocrine function (Fig. 2G,I).

Slow pressor AngII increases SBP in males but not in females

Two-way ANOVA analysis of SBP on day 13, showed a main effect of sex [$F(1,36)=4.58$, $p < .05$] and a marginally significant AngII condition X sex interaction [$F(1,36)=3.92$, $p=.055$] (Fig. 3A,B). Post hoc analysis revealed that, across conditions, SBP was greater in males

(124.2 ± 3.7) than females (112.2 ± 4.1; p < .05), and that, consistent with previous studies (Coleman et al., 2013; Marques-Lopes et al., 2014; Wang et al., 2013; Xue et al., 2005), infusion of AngII increased SBP in males (134.1 ± 6.5) relative to saline controls (116.7 ± 4.7). This effect was not observed in females ($p < .05$). No differences in SBP were found in all other timepoints.

Slow-pressor AngII increases ROS production in males but not in females

ROS production in the PVN has been suggested to play a causative role in AngII-induced hypertension and to be associated with increased NMDA receptor activity (Erdos et al., 2006; Wang et al., 2013). Therefore, baseline (prior to NMDA application) and NMDA-evoked ROS production was analyzed by fluorescence imaging in dissociated AT1aR-EGFP PVN cells (Fig. 4A). Main effects of AngII condition [$F(1,41)=5.32$, $p < .05$], sex [$F(1,41)=5.43$, $p < .05$] and NMDA administration [$F(1,41)=20.84$, $p < .001$] were found (Fig. 4A–B). Moreover, marginally significant NMDA administration X sex [$F(1,41)=3.69$, $p = .062$] and NMDA administration X AngII condition [$F(1,41)=3.61$, $p = .065$] interactions also were found (Fig. 4B). Post hoc analysis revealed that, across sexes, AngII infusion increased ROS production (95.05 ± 2.64) relative to saline controls (85.98 ± 2.91, $p < .05$); that, across conditions, males had greater ROS production (95.10 ± 2.59) than females (85.94 ± 2.96, $p < .05$); and that NDMA administration increased ROS production (93.37 ± 2.45) in comparison with baseline levels (87.66 ± 1.58, $p < .001$). Moreover, we observed that NMDA application induced a greater increase in ROS production in males than in females ($p = .062$), and in AngII-infused mice than in saline controls ($p = .065$).

In AT1aR-EGFP dendrites, slow-pressor AngII infusion increases GluN1 density in male and female mice

Two-way ANOVA analysis showed a marginally significant [$F(1,153)=3.78$, $p=.054$] effect of AngII condition in near plasmalemmal GluN1-SIG density in AT1aR-EGFP-containing dendrites (Fig. 5A–D and 6B). Furthermore, a main effect of AngII condition was found in cytoplasmic [$F(1,567)=36.51$, $p < .01$] and total [$F(1,643)=52.95$, $p < .001$] GluN1-SIG densities (Fig. 5A–D and 6C–D). Post hoc analysis revealed that, across sexes, AngII infusion increased near plasmalemmal (0.30 ± 0.01), cytoplasmic (1.98 ± 0.07) and total (2.38 ± 0.08) GluN1-SIG densities in comparison with saline controls (near plasmalemmal: 0.27 ± 0.01, $p = .054$; cytoplasmic: 1.43 ± 0.06, $p < .001$; total: 1.63 ± 0.07, $p < .001$). No effects were found in plasmalemmal GluN1-SIG density.

GluN1-SIG density was further analyzed in small and large dendrites, which correspond to distal and proximal dendrites, respectively (Peters et al., 1991). In small AT1aR-EGFP dendrites, a main effect of AngII condition was found in cytoplasmic [$F(1,466)=31.92$, $p < .01$] GluN1-SIG density (Fig. 7A). Post hoc analysis revealed that, across sexes, AngII infusion increased cytoplasmic (2.17 ± 0.07) GluN1-SIG density in comparison with saline controls (1.59 ± 0.07, $p < .001$). Furthermore, main effects of AngII condition [$F(1,531)=41.86$, $p < .01$] and sex [$F(1,531)=5.36$, $p < .05$] were found in total GluN1-SIG density. Post hoc analysis revealed that, across sexes, AngII infusion increased total (2.65 ± 0.09) GluN1-SIG density in comparison with saline controls (1.87 ± 0.08, $p < .001$), and that, across conditions, females (2.40 ± 0.09) had greater cytoplasmic GluN1-SIG density

than males (2.12 ± 0.09, $p < .05$). (Fig. 7B). No differences were found in plasmalemmal and near plasmalemmal GluN1-SIG densities.

In large AT1aR-EGFP dendrites, a main effect of AngII condition [cytoplasmic: $F(1,81)=8.18$, $p < .01$; total: $F(1,98)=15.11$, $p < .001$] and a significant AngII condition X sex interaction [cytoplasmic: $F(1,81)=10.22$, $p < .01$; total: $F(1,98)=7.45$, $p < .01$] were found in cytoplasmic and total GluN1-SIG densities (Fig. 7C–D). Post hoc analysis revealed that, across sexes, AngII infusion increased cytoplasmic and total GluN1-SIG densities (cytoplasmic: 0.99 ± 0.09; total 1.20 ± 0.01) relative to saline controls (cytoplasmic: 0.64 ± 0.08, $p < .01$; total: 0.70 ± 0.09, $p < .001$), and that AngII infusion induced cytoplasmic and total GluN1-SIG densities increases in females (cytoplasmic 1.24 ± 0.17; total: 1.50 ± 0.19) relative to saline controls (cytoplasmic 0.49 ± 0.05; total: 0.64 ± 0.06). These effects were not observed in males ($p < .01$ for both) (Figs. 7C–D). No differences were found in plasmalemmal and near plasmalemmal GluN1-SIG densities.

In AT1aR-EGFP dendrites, slow pressor AngII infusion induces increases in cytoplasmic and total GluN1-SIG counts in males and females

GluN1-SIG counts were performed in PVN AT1aR-EGFP dendrites to evaluate if the AngII-induced increases in GluN1-SIG density in males and females were due to morphological changes. In cytoplasmic and total GluN1-SIG counts, there were main effects of AngII condition [cytoplasmic: $F(1,604)=44.52$, $p < .001$; total: $F(1,632)=87.78$, $p < .001$] and sex [cytoplasmic: $F(1,604)=21.12$, $p < .001$; total; $F(1,632)=9.38$, $p < .01$], and significant AngII condition X sex interactions [cytoplasmic: $F(1,604)=22.43$, $p < .001$; total: $F(1,632)=44.52$, $p < .01$] (Figs. 8C–D). Post hoc analysis revealed that, across sexes, AngII infusion increased cytoplasmic (2.10 ± 0.06) and total (2.34 ± 0.06) GluN1-SIG counts relative to saline controls (cytoplasmic: 1.54 ± 0.06, $p < .001$; total: 1.54 ± 0.06, $p < .001$), and that, across conditions, females (cytoplasmic: 2.01 ± 0.06; total: 2.07 ± 0.06) had greater GluN1-SIG counts than males (cytoplasmic: 1.62 ± 0.06, $p < .001$; total: 1.81 ± 0.06, $p < .01$). Moreover, we observed that AngII infusion induced greater cytoplasmic (2.30 ± 0.12) and total (2.61 ± 0.13) GluN1-SIG densities increases in females relative to saline controls (cytoplasmic 1.24 ± 0.04; total: 1.53 ± 0.05) than in males (AngII: cytoplasmic 1.70 ± 0.09; total: 2.06 ± 0.09/saline: cytoplasmic 1.43 ± 0.05, $p < .001$; total: 1.56 ± 0.06, $p < .01$). No differences were found in plasmalemmal and near plasmalemmal GluN1-SIG counts.

In AT1aR-EGFP dendrites, slow pressor AngII infusion induces differential morphological changes in males and females

In all (small plus large) AT1aR-EGFP dendrites in the PVN, significant AngII condition X sex interactions were found in dendritic area [$F(1,634)=7.99$, $p < .01$] and diameter [$F(1,629)=9.89$, $p < .01$] (Fig. 9A–B). Post hoc analysis showed dendritic area was increased by AngII infusion in females (AngII: 1.20 ± 0.05; saline: 1.07 ± 0.05), but decreased males (AngII: 1.01 ± 0.04; saline: 1.15 ± 0.05, $p < .01$), relative to saline controls. Moreover, AngII infusion decreased dendritic diameter in males (AngII: 0.70 ± 0.01; saline: 0.78 ± 0.02), but induced no change in females ($p < .01$), relative to saline controls.

In small AT1aR-EGFP dendrites, a main effect of sex [$F(1,326)=4.26$, $p < .05$] was found in dendritic area. Moreover, significant AngII condition X sex interactions were found in dendritic area [$F(1,326)=11.98$, $p < .01$] and diameter [$F(1,544)=8.79$, $p < .01$] (Fig. 9C–D). Post hoc analysis showed that, across conditions, dendritic area was greater in males (0.70 ± 0.01) than in females (0.65 ± 0.01, $p < .05$), and that dendritic area was increased by AngII infusion in females (AngII: 0.68 ± 0.02; saline: 0.62 ± 0.02), but decreased in males (AngII: 0.66 ± 0.02; saline: 0.73 ± 0.02, $p < .01$), relative to saline controls. Moreover, AngII infusion decreased dendritic diameter in males (AngII: 0.67 ± 0.01; saline: 0.73 ± 0.01), but induced no change in females ($p < .01$), relative to saline controls.

In large AT1aR-EGFP dendrites, no effects were observed in dendritic area (Fig. 9E). However, a main effect of AngII condition was found in dendritic diameter [$F(1,100)=13.58$, $p < .001$] (Fig. 9F). Post hoc analysis showed that, across sexes, AngII infusion decreased dendritic diameter (1.12 ± 0.03), relative to saline controls (1.24 ± 0.02, $p < .001$).

DISCUSSION

This study demonstrates that in males, but not in females, AngII induces increases in SBP and in ROS production both at baseline and following NMDA application in PVN AT1aR-EGFP cells. We also show that while AngII enhanced cytoplasmic and total GluN1 densities in both sexes, in females AngII elicited a greater increase in cytoplasmic and total GLuN1 densities in large AT1aR-EGFP dendrites than in males (Fig. 10). These results suggest that sex differences in AngII-induced hypertension are associated with augmented ROS production in AT1aR-containing PVN cells in males, but not with differential post-synaptic NMDA receptor trafficking in these cells. Our results also suggest that these effects are not likely the result of estrogen signaling in AT1aR-containing cells.

Labeling of EGFP and GluN1 in the PVN

As previously described (Gonzalez et al., 2012), neither the morphology nor the number of AT1aR-EGFP-labeled cells differed in the PVN of males and females. We also observed many extrasynaptic plasmalemmal NMDA receptors, which are thought to contain NR2B subunits (Petralia et al., 2009). Extrasynaptic NMDA receptors are thought to be activated by glutamate spillover from the synapse or ectopic release of glutamate from adjacent processes and have been suggested to be awaiting incorporation into the synapse through lateral diffusion within the plasma membrane (Petralia, 2012; Wenthold et al., 2003). Cytoplasmic NMDA receptors can be transported to the plasmalemma after receptor assembly in the endoplasmic reticulum and processing in the Golgi apparatus (Wenthold et al., 2003). While endocytosis of NMDA receptors may preferentially occur away from the synapse (Nong et al., 2004), near plasmalemmal GluN1 may represent functional NMDA receptors in transit to or from the plasma membrane.

AT1aR and spinal cord

Our findings demonstrate that in the mouse, AT1aR-containing neurons in the PVN do not project to the spinal cord, in agreement with work by Oldfield et al. (2001) in rat,

highlighting that indirect pathways may mediate the effect of AngII on blood pressure via AT1 receptors in the PVN. AT1 receptor-containing PVN neurons have direct projections to presympathetic neurons of the rostral ventrolateral medulla (RVLM; Cato and Toney, 2005) and parabrachial nucleus (Fink et al., 1991). While such projections may convey glutamatergic input from AT1aR-containing PVN neurons to influence blood pressure (Fulwiler and Saper, 1984), AT1 receptor-mediated effects may occur within the PVN. For example, Latchford and Ferguson (2004) demonstrated increases in glutamatergic input to magnocellular PVN neurons following AngII, and AT1 receptors may mediate presynaptic modulation of spinally projecting PVN neurons (Li et al., 2003). Thus, the substantial anatomical overlap in populations of AT1aR-containing and FG-labeled, spinally projecting neurons supports the possibility of an intra-PVN pathway facilitating modulation of blood pressure by AT1 receptors.

AT1aR are mostly expressed in non-neuroendocrine neurons of the PVN

As in previous studies in mice (Gonzalez et al., 2012) and rats (Egli et al., 2000; Lenkei et al., 1995), AT1aR and AVP are expressed in different cell populations in the PVN. While in mice neuroendocrine neurons, such as AVP-containing neurons, are distributed throughout the parvicellular and magnocellular subregions of the PVN (Biag et al., 2012), AVP is predominately located in magnocellular neurons (Coleman et al., 2009), characterized by endocrine projections to blood-brain barrier-deprived median eminence and posterior pituitary (Swanson and Kuypers, 1980; Swanson and Sawchenko, 1980). Oldfield et al. (2001) demonstrated the expression of AT1 receptors in median eminence-projecting parvicellular PVN neurons in rats. Therefore, the observed FG-labeled AT1aR-EGFP-containing PVN cells in our study might be neuroendocrine parvicellular neurons projecting to the median eminence.

Sex differences in slow pressor AngII-induced hypertension—As others have reported (Girouard et al., 2009; Marques-Lopes et al., 2014; Xue et al., 2013a; Xue et al., 2005), AngII infusion-elicited blood pressure increases in young males but not young females suggests a protective role of estrogen. Central, but not peripheral, estrogen receptor blockade results in increased blood pressure in intact female mice (Xue et al., 2007). Moreover, the interaction of estrogens with the RAS may further contribute to inhibition of central AngII pressor effects (Kisley et al., 1999; Rosas-Arellano et al., 1999; Tanaka et al., 2001). In particular, estrogens decrease expression of pro-hypertensive AT1 receptor and angiotensin-converting enzyme 1, and increases expression of anti-hypertensive Mas receptor and angiotensin-converting enzyme 2 in the rat lamina terminalis (Xue et al., 2014). Therefore, the observed sex difference in AngII-induced hypertension may be due to estrogen protective effect in females.

Sex differences in AngII-induced ROS production in PVN AT1aR-EGFP cells—Our findings of AngII-associated increased ROS production at baseline and after NMDA application in PVN AT1aR-EGFP cells in male, but not female mice are in agreement with previous studies showing increased ROS production that is NADPH oxidase-dependent in the PVN of AngII-infused male mice (Braga et al., 2011; Coleman et al., 2013; Jancovski et al., 2013; Wang et al., 2013). In the PVN of male mice, AngII infusion is associated with

increased co-localization of GluN1 with NADPH oxidase-containing dendrites and increased density of critical near plasmalemmal NADPH oxidase subunits in non-AVP containing dendrites, concomitant with both increased ROS production and NMDA receptor activity (Coleman et al., 2013; Wang et al., 2013). Intriguingly, recent data from our lab shows opposite findings in female mice, as near plasmalemmal NADPH oxidase density is decreased in non-AVP-containing PVN dendrites following AngII infusion (Van Kempen et al., unpublished data). Taken together with the absence of AT1aR and AVP co-localization in the mouse PVN (Gonzalez et al., 2012), the present results suggest that opposing changes in NADPH oxidase density could contribute to enhanced ROS production in males, but not in females. In addition, estrogen could play a role in the protection from ROS production increases in AT1aR-containing PVN cells, as previous studies showed estrogen-mediated prevention of ROS increases in SFO slices from AngII-infused male mice (Xue et al., 2008). Of note, as NADPH oxidase also is expressed in PVN glial cells (Coleman et al., 2013), the observed ROS in our study may also arise from non-neuronal cells.

AT1aR are not expressed in ERβ-containing PVN neurons

Although AT1aR and ERβ are thought to be expressed in the parvicellular population we did not find PVN neurons containing immunoreactivity for both AT1aR-eGFP and ERβ immunoreactivity in the PVN, as demonstrated in rats (Gonzalez et al., 2012; Hauser et al., 1998; Laflamme et al., 1998; Lenkei et al., 1997; Milner et al., 2010). Nevertheless, estrogen could regulate AT1aR-containing PVN neurons via afferents arising from ER-expressing areas, including the SFO (Tanaka et al., 2001; Xue et al., 2009) and the NTS (Ricardo and Koh, 1978; Shughrue and Merchenthaler, 2001). In addition, although recent work by Xue et al. (2013b) showed that ERα in the rat PVN does not confer protection from aldosterone-induced hypertension, estrogen could modulate AT1aR-expressing neurons through ERα. Conceivably, ERβ may be co-localized with AT1bR, whose mRNA distribution in the mouse PVN is similar to AT1aR (Chen et al., 2003; Zhou et al., 2005). Thus, although AT1aR-containing PVN dendrites of AngII-infused females do not show protection from GluN1 density changes, the absence of increased ROS production in AT1aR-expressing PVN cells may be due to estrogen-mediated protection that prevents increases in blood pressure. In addition, greater levels of neuronal nitric oxide synthase in the SFO and PVN of female mice in comparison to males both pre- and post-AngII infusion (Xue et al., 2009) could also prevent hypertension despite the changes in NMDA receptor trafficking.

Slow pressor AngII infusion induces changes in dendritic density of GluN1 in PVN neurons containing AT1aR-EGFP—AngII infusion-induced changes in post-synaptic GluN1 density and subcellular localization in AT1aR-EGFP neurons in the PVN of male and female mice suggests enhanced synthesis and/or decreased degradation of GluN1. Near plasmalemmal accumulation of GluN1 may result from desensitization/internalization of NMDA receptors in response to repetitive activation (Nakamichi and Yoneda, 2005). Together with increased total GluN1 density, this suggests that internalized GluN1 may be recycled to the plasma membrane rather than being degraded, similar to our previous findings in ERβ-containing PVN dendrites of males and aged female mice with concomitant blood pressure elevation (Marques-Lopes et al., 2014). In accordance, enhanced PVN post-synaptic NMDA receptor activity is associated with increased sympathoexcitation in

hypertensive rats and mice (Bardgett et al., 2014; Li and Pan, 2010; Li et al., 2008; Li et al., 2014; Wang et al., 2013; Ye et al., 2012).

Our results also show that AngII induces a greater increase in cytoplasmic and total GluN1 densities in proximal AT1aR-containing PVN dendrites of females than in males. Likewise, AngII induces a greater increase in post-synaptic cytoplasmic and total SIG counts in all AT1aR-expressing PVN neurons of females than in males. Together with the lack of sex differences in plasmalemmal and near plasmalemmal GluN1 densities, these results suggest that although the increase in GluN1 expression in response to AngII is greater in females than in males, there is no difference in trafficking to the plasma membrane and therefore in amount of receptor available for ligand binding. Work by Huh and Wenthold (1999) showed that, if unassembled with GluN2, the GluN1 cytoplasmic pool is degraded. Therefore, these results suggest that the AngII-driven sexual dimorphic changes in GluN1 density in AT1aR-containing PVN dendrites are independent of the changes in BP and ROS production. Importantly, altered cytoplasmic and total GluN1 density in PVN AT1aR-expressing dendrites of AngII-infused males and females were not due to changes in dendritic area, since the same differences were observed comparing the numbers of GluN1-SIG particles.

Sex differences in AngII-induced morphological changes in PVN AT1aR-EGFP dendrites—The AngII-elicited morphological changes in PVN AT1aR-EGFP-expressing dendrites in males and females are reminiscent of changes in dendritic spine density and in dendritic morphology that have been reported in diverse hypertension models in rats (Aicher et al., 2003; Dyball and Garten, 1988; Sanchez et al., 2011; Tang et al., 1995; Vega et al., 2004). In particular, Aicher et al. (2003) showed changes in number and structure of glutamatergic dendritic spines in the NTS of SHR, which, in agreement with our findings, suggests that altered afferent activity in hypertension induces post-synaptic changes in glutamatergic neurons

Gonadal hormones play a key role in inducing morphological changes in dendrites. Androgen- and estrogen-driven effects in dendritic density and morphology have been shown in the CA1 region of the dorsal hippocampus, ventromedial nucleus of the hypothalamus, and medial nucleus of the amygdala (Cooke and Woolley, 2005; Madeira et al., 2001; McEwen, 1994; Shors et al., 2001). In particular, estrogen-elicited dendritic spine plasticity has been shown in hippocampal and hypothalamic non-ER-containing neurons, suggesting an indirect (i.e. trans-synaptic) mechanism (Cooke and Woolley, 2005). Therefore, similarly to ROS production, the differential AngII-evoked morphological effects in AT1aR--expressing dendrites in males and females could be due to estrogen mediation.

In conclusion, our results show that AngII infusion increases blood pressure and ROS production in AT1aR-containing PVN neurons of males, but not females. However, no sex differences are observed in AngII-induced changes in GluN1 density in AT1aR-expressing dendrites in the PVN. Furthermore, we show that AT1aR-containing neurons do not project to the spinal cord and that AT1aR and ERβ do not co-localize in the mouse PVN. Therefore, our results suggest that estrogen could play a protective role against hypertension in females by preventing sympathoexcitation associated with increased ROS production in AT1aR-

expressing PVN neurons, but not increased post-synaptic NMDA receptor density in this neuronal population.

Acknowledgments

GRANT SUPPORT: NIH grants HL098351, DA08259 & AG016765 (TAM), HL096571 (CI, VMP, TAM), AG059850 (EMW), T32 DA007274 (TAV)

We would like to thank Andreina Gonzalez, Sanoara Mazid, Eugene Ogorodnik and Vladimir Mudragel for their excellent technical assistance.

References

Aguilera G, Young WS, Kiss A, Bathia A. Direct regulation of hypothalamic corticotropin-releasing-hormone neurons by angiotensin II. Neuroendocrinology. 1995; 61(4):437–444. [PubMed: 7783857]

Aicher SA, Sharma S, Mitchell JL. Structural changes in AMPA-receptive neurons in the nucleus of the solitary tract of spontaneously hypertensive rats. Hypertension. 2003; 41(6):1246–1252. [PubMed: 12695422]

Bardgett ME, Chen QH, Guo Q, Calderon AS, Andrade MA, Toney GM. Coping with Dehydration: Sympathetic Activation and Regulation of Glutamatergic Transmission in the Hypothalamic PVN. American Journal of Physiology Regulatory, Integrative and Comparative Physiology. 2014

Beckerman MA, Glass MJ. The NMDA-NR1 receptor subunit and the mu-opioid receptor are expressed in somatodendritic compartments of central nucleus of the amygdala neurons projecting to the bed nucleus of the stria terminalis. Experimental Neurology. 2012; 234(1):112–126. [PubMed: 22227057]

Biag J, Huang Y, Gou L, Hintiryan H, Askarinam A, Hahn JD, Toga AW, Dong HW. Cyto- and chemoarchitecture of the hypothalamic paraventricular nucleus in the C57BL/6J male mouse: a study of immunostaining and multiple fluorescent tract tracing. The Journal of Comparative Neurology. 2012; 520(1):6–33. [PubMed: 21674499]

Biancardi VC, Son SJ, Ahmadi S, Filosa JA, Stern JE. Circulating angiotensin II gains access to the hypothalamus and brain stem during hypertension via breakdown of the blood-brain barrier. Hypertension. 2014; 63(3):572–579. [PubMed: 24343120]

Braga VA, Medeiros IA, Ribeiro TP, Franca-Silva MS, Botelho-Ono MS, Guimaraes DD. Angiotensin-II-induced reactive oxygen species along the SFO-PVN-RVLM pathway: implications in neurogenic hypertension. Brazilian Journal of Medical and Biological Research = Revista brasileira de pesquisas medicas e biologicas/Sociedade Brasileira de Biofisica [et al]. 2011; 44(9): 871–876.

Cato MJ, Toney GM. Angiotensin II excites paraventricular nucleus neurons that innervate the rostral ventrolateral medulla: an in vitro patch-clamp study in brain slices. Journal of Neurophysiology. 2005; 93(1):403–413. [PubMed: 15356186]

Chen Y, da Rocha MJ, Morris M. Osmotic regulation of angiotensin AT1 receptor subtypes in mouse brain. Brain Research. 2003; 965(1–2):35–44. [PubMed: 12591117]

Coleman CG, Anrather J, Iadecola C, Pickel VM. Angiotensin II type 2 receptors have a major somatodendritic distribution in vasopressin-containing neurons in the mouse hypothalamic paraventricular nucleus. Neuroscience. 2009; 163(1):129–142. [PubMed: 19539723]

Coleman CG, Wang G, Faraco G, Marques Lopes J, Waters EM, Milner TA, Iadecola C, Pickel VM. Membrane trafficking of NADPH oxidase p47(phox) in paraventricular hypothalamic neurons parallels local free radical production in angiotensin II slow-pressor hypertension. The Journal of Neuroscience: the official journal of the Society for Neuroscience. 2013; 33(10):4308–4316. [PubMed: 23467347]

Coleman CG, Wang G, Park L, Anrather J, Delagrammatikas GJ, Chan J, Zhou J, Iadecola C, Pickel VM. Chronic intermittent hypoxia induces NMDA receptor-dependent plasticity and suppresses nitric oxide signaling in the mouse hypothalamic paraventricular nucleus. The Journal of

Neuroscience: the official journal of the Society for Neuroscience. 2010; 30(36):12103–12112. [PubMed: 20826673]

Cooke BM, Woolley CS. Gonadal hormone modulation of dendrites in the mammalian CNS. Journal of Neurobiology. 2005; 64(1):34–46. [PubMed: 15884004]

Creutz LM, Kritzer MF. Estrogen receptor-beta immunoreactivity in the midbrain of adult rats: regional, subregional, and cellular localization in the A10, A9, and A8 dopamine cell groups. The Journal of Comparative Neurology. 2002; 446(3):288–300. [PubMed: 11932944]

Drouyer E, LeSauter J, Hernandez AL, Silver R. Specializations of gastrin-releasing peptide cells of the mouse suprachiasmatic nucleus. The Journal of Comparative Neurology. 2010; 518(8):1249–1263. [PubMed: 20151358]

Dyball RE, Garten LL. Stimulus-related changes in the dendrites of magnocellular neurones. Brain Research Bulletin. 1988; 20(6):675–680. [PubMed: 3409052]

Egli M, Laurent JP, Mosimann R, Felix D, Imboden H. Morphological and immunocytochemical characterization of electrophysiologically investigated neurons in the PVN of the rat. Journal of Neuroscience Methods. 2000; 95(2):145–150. [PubMed: 10752485]

Encinas JM, Vaahtokari A, Enikolopov G. Fluoxetine targets early progenitor cells in the adult brain. Proceedings of the National Academy of Sciences of the United States of America. 2006; 103(21):8233–8238. [PubMed: 16702546]

Erdos B, Broxson CS, King MA, Scarpace PJ, Tumer N. Acute pressor effect of central angiotensin II is mediated by NAD(P)H-oxidase-dependent production of superoxide in the hypothalamic cardiovascular regulatory nuclei. Journal of Hypertension. 2006; 24(1):109–116. [PubMed: 16331108]

Ferguson AV. Angiotensinergic regulation of autonomic and neuroendocrine outputs: critical roles for the subfornical organ and paraventricular nucleus. Neuroendocrinology. 2009; 89(4):370–376. [PubMed: 19342823]

Ferguson AV, Latchford KJ. Local circuitry regulates the excitability of rat neurohypophysial neurones. Experimental Physiology. 2000; 85(Spec No):153S–161S. [PubMed: 10795918]

Fink GD, Pawloski CM, Ohman LE, Haywood JR. Lateral parabrachial nucleus and angiotensin II-induced hypertension. Hypertension. 1991; 17(6 Pt 2):1177–1184. [PubMed: 1675203]

Freeman KL, Brooks VL. AT(1) and glutamatergic receptors in paraventricular nucleus support blood pressure during water deprivation. American Journal of Physiology Regulatory, Integrative and Comparative Physiology. 2007; 292(4):R1675–1682.

Fulwiler CE, Saper CB. Subnuclear organization of the efferent connections of the parabrachial nucleus in the rat. Brain Research. 1984; 319(3):229–259. [PubMed: 6478256]

Gabor A, Leenen FH. Cardiovascular effects of angiotensin II and glutamate in the PVN of Dahl salt-sensitive rats. Brain Research. 2012a; 1447:28–37. [PubMed: 22356885]

Gabor A, Leenen FH. Central neuromodulatory pathways regulating sympathetic activity in hypertension. Journal of Applied Physiology. 2012b; 113(8):1294–1303. [PubMed: 22773773]

Gabor A, Leenen FH. Central mineralocorticoid receptors and the role of angiotensin II and glutamate in the paraventricular nucleus of rats with angiotensin II-induced hypertension. Hypertension. 2013; 61(5):1083–1090. [PubMed: 23509081]

Girouard H, Wang G, Gallo EF, Anrather J, Zhou P, Pickel VM, Iadecola C. NMDA receptor activation increases free radical production through nitric oxide and NOX2. The Journal of Neuroscience: the official journal of the Society for Neuroscience. 2009; 29(8):2545–2552. [PubMed: 19244529]

Glass MJ, Robinson DC, Waters E, Pickel VM. Deletion of the NMDA-NR1 receptor subunit gene in the mouse nucleus accumbens attenuates apomorphine-induced dopamine D1 receptor trafficking and acoustic startle behavior. Synapse. 2013; 67(6):265–279. [PubMed: 23345061]

Gong S, Zheng C, Doughty ML, Losos K, Didkovsky N, Schambra UB, Nowak NJ, Joyner A, Leblanc G, Hatten ME, Heintz N. A gene expression atlas of the central nervous system based on bacterial artificial chromosomes. Nature. 2003; 425(6961):917–925. [PubMed: 14586460]

Gonzalez AD, Wang G, Waters EM, Gonzales KL, Speth RC, Van Kempen TA, Marques-Lopes J, Young CN, Butler SD, Davisson RL, Iadecola C, Pickel VM, Pierce JP, Milner TA. Distribution

of angiotensin type 1a receptor-containing cells in the brains of bacterial artificial chromosome transgenic mice. Neuroscience. 2012; 226:489–509. [PubMed: 22922351]

Hashimoto K, Nishiyama M, Tanaka Y, Noguchi T, Asaba K, Hossein PN, Nishioka T, Makino S. Urocortins and corticotropin releasing factor type 2 receptors in the hypothalamus and the cardiovascular system. Peptides. 2004; 25(10):1711–1721. [PubMed: 15476938]

Hauser W, Johren O, Saavedra JM. Characterization and distribution of angiotensin II receptor subtypes in the mouse brain. European Journal of Pharmacology. 1998; 348(1):101–114. [PubMed: 9650837]

Huh KH, Wenthold RJ. Turnover analysis of glutamate receptors identifies a rapidly degraded pool of the N-methyl-D-aspartate receptor subunit, NR1, in cultured cerebellar granule cells. The Journal of Biological Chemistry. 1999; 274(1):151–157. [PubMed: 9867823]

Hundahl CA, Hannibal J, Fahrenkrug J, Dewilde S, Hay-Schmidt A. Neuroglobin expression in the rat suprachiasmatic nucleus: colocalization, innervation, and response to light. The Journal of Comparative Neurology. 2010; 518(9):1556–1569. [PubMed: 20187147]

Jancovski N, Bassi JK, Carter DA, Choong YT, Connelly A, Nguyen TP, Chen D, Lukoshkova EV, Menuet C, Head GA, Allen AM. Stimulation of angiotensin type 1A receptors on catecholaminergic cells contributes to angiotensin-dependent hypertension. Hypertension. 2013; 62(5):866–871. [PubMed: 24001896]

Jinno S, Kosaka T. Immunocytochemical characterization of hippocamposeptal projecting GABAergic nonprincipal neurons in the mouse brain: a retrograde labeling study. Brain Research. 2002; 945(2):219–231. [PubMed: 12126884]

Kisley LR, Sakai RR, Fluharty SJ. Estrogen decreases hypothalamic angiotensin II AT1 receptor binding and mRNA in the female rat. Brain Research. 1999; 844(1–2):34–42. [PubMed: 10536259]

Laflamme N, Nappi RE, Drolet G, Labrie C, Rivest S. Expression and neuropeptidergic characterization of estrogen receptors (ERalpha and ERbeta) throughout the rat brain: anatomical evidence of distinct roles of each subtype. Journal of Neurobiology. 1998; 36(3):357–378. [PubMed: 9733072]

Latchford KJ, Ferguson AV. ANG II-induced excitation of paraventricular nucleus magnocellular neurons: a role for glutamate interneurons. American Journal of Physiology Regulatory, Integrative and Comparative Physiology. 2004; 286(5):R894–902.

Lenkei Z, Corvol P, Llorens-Cortes C. Comparative expression of vasopressin and angiotensin type-1 receptor mRNA in rat hypothalamic nuclei: a double in situ hybridization study. Brain Research Molecular Brain Research. 1995; 34(1):135–142. [PubMed: 8750869]

Lenkei Z, Palkovits M, Corvol P, Llorens-Cortes C. Expression of angiotensin type-1 (AT1) and type-2 (AT2) receptor mRNAs in the adult rat brain: a functional neuroanatomical review. Frontiers in Neuroendocrinology. 1997; 18(4):383–439. [PubMed: 9344632]

Li DP, Chen SR, Pan HL. Angiotensin II stimulates spinally projecting paraventricular neurons through presynaptic disinhibition. The Journal of Neuroscience: the official journal of the Society for Neuroscience. 2003; 23(12):5041–5049. [PubMed: 12832527]

Li DP, Pan HL. Increased group I metabotropic glutamate receptor activity in paraventricular nucleus supports elevated sympathetic vasomotor tone in hypertension. American Journal of Physiology Regulatory, Integrative and Comparative Physiology. 2010; 299(2):R552–561.

Li DP, Yang Q, Pan HM, Pan HL. Pre- and postsynaptic plasticity underlying augmented glutamatergic inputs to hypothalamic presympathetic neurons in spontaneously hypertensive rats. The Journal of Physiology. 2008; 586(6):1637–1647. [PubMed: 18238817]

Li DP, Zhu LH, Pachuau J, Lee HA, Pan HL. mGluR5 Upregulation Increases Excitability of Hypothalamic Presympathetic Neurons through NMDA Receptor Trafficking in Spontaneously Hypertensive Rats. The Journal of Neuroscience: the official journal of the Society for Neuroscience. 2014; 34(12):4309–4317. [PubMed: 24647951]

Lind RW, Van Hoesen GW, Johnson AK. An HRP study of the connections of the subfornical organ of the rat. The Journal of Comparative Neurology. 1982; 210(3):265–277. [PubMed: 7142442]

Madeira MD, Ferreira-Silva L, Paula-Barbosa MM. Influence of sex and estrus cycle on the sexual dimorphisms of the hypothalamic ventromedial nucleus: stereological evaluation and Golgi study. The Journal of Comparative Neurology. 2001; 432(3):329–345. [PubMed: 11246211]

Marques-Lopes J, Van Kempen T, Waters EM, Pickel VM, Iadecola C, Milner TA. Slow-pressor angiotensin II hypertension and concomitant dendritic NMDA receptor trafficking in estrogen receptor beta-containing neurons of the mouse hypothalamic paraventricular nucleus are sex and age dependent. The Journal of Comparative Neurology. 2014

Martins D, Nelson K, Pan D, Tareen N, Norris K. The effect of gender on age-related blood pressure changes and the prevalence of isolated systolic hypertension among older adults: data from NHANES III. The Journal of Gender-Specific Medicine: JGSM: the official journal of the Partnership for Women's Health at Columbia. 2001; 4(3):10–13. 20.

McEwen BS. How do sex and stress hormones affect nerve cells? Annals of the New York Academy of Sciences. 1994; 743:1–16. discussion 17–18. [PubMed: 7802409]

Milner TA, Thompson LI, Wang G, Kievits JA, Martin E, Zhou P, McEwen BS, Pfaff DW, Waters EM. Distribution of estrogen receptor beta containing cells in the brains of bacterial artificial chromosome transgenic mice. Brain Research. 2010; 1351:74–96. [PubMed: 20599828]

Milner TA, Waters EM, Robinson DC, Pierce JP. Degenerating processes identified by electron microscopic immunocytochemical methods. Methods in Molecular Biology. 2011; 793:23–59. [PubMed: 21913092]

Miselis RR. The efferent projections of the subfornical organ of the rat: a circumventricular organ within a neural network subserving water balance. Brain Research. 1981; 230(1–2):1–23. [PubMed: 7317773]

Nakamichi N, Yoneda Y. Functional proteins involved in regulation of intracellular Ca(2+) for drug development: desensitization of N-methyl-D-aspartate receptor channels. Journal of pharmacological sciences. 2005; 97(3):348–350. [PubMed: 15764843]

Nong Y, Huang YQ, Salter MW. NMDA receptors are movin' in. Current Opinion in Neurobiology. 2004; 14(3):353–361. [PubMed: 15194116]

Nunn N, Womack M, Dart C, Barrett-Jolley R. Function and pharmacology of spinally-projecting sympathetic pre-autonomic neurones in the paraventricular nucleus of the hypothalamus. Current Neuropharmacology. 2011; 9(2):262–277. [PubMed: 22131936]

O'Callaghan EL, Choong YT, Jancovski N, Allen AM. Central angiotensinergic mechanisms associated with hypertension. Autonomic Neuroscience: Basic & Clinical. 2013; 175(1–2):85–92. [PubMed: 23466041]

Oldfield BJ, Davern PJ, Giles ME, Allen AM, Badoer E, McKinley MJ. Efferent neural projections of angiotensin receptor (AT1) expressing neurones in the hypothalamic paraventricular nucleus of the rat. Journal of Neuroendocrinology. 2001; 13(2):139–146. [PubMed: 11168839]

Paton JF, Wang S, Polson JW, Kasparov S. Signalling across the blood brain barrier by angiotensin II: novel implications for neurogenic hypertension. Journal of Molecular Medicine. 2008; 86(6):705–710. [PubMed: 18443753]

Perello M, Raingo J. Leptin activates oxytocin neurons of the hypothalamic paraventricular nucleus in both control and diet-induced obese rodents. PloS one. 2013; 8(3):e59625. [PubMed: 23527232]

Peters, A.; Palay, S.; Webster, H. The fine structure of the nervous system. New York: Oxford UP; 1991.

Petralia RS. Distribution of extrasynaptic NMDA receptors on neurons. The Scientific World Journal. 2012; 2012:267120.

Petralia, RS.; Al-Hallaq, RA.; Wenthold, RJ. Trafficking and Targeting of NMDA Receptors. In: Van Dongen, AM., editor. Biology of the NMDA Receptor. Boca Raton (FL): 2009.

Pierce JP, Kievits J, Graustein B, Speth RC, Iadecola C, Milner TA. Sex differences in the subcellular distribution of angiotensin type 1 receptors and NADPH oxidase subunits in the dendrites of C1 neurons in the rat rostral ventrolateral medulla. Neuroscience. 2009; 163(1):329–338. [PubMed: 19501631]

Pierce JP, Kurucz OS, Milner TA. Morphometry of a peptidergic transmitter system: dynorphin B-like immunoreactivity in the rat hippocampal mossy fiber pathway before and after seizures. Hippocampus. 1999; 9(3):255–276. [PubMed: 10401641]

Polgar E, Thomson S, Maxwell DJ, Al-Khater K, Todd AJ. A population of large neurons in laminae III and IV of the rat spinal cord that have long dorsal dendrites and lack the neurokinin 1 receptor. The European Journal of Neuroscience. 2007; 26(6):1587–1598. [PubMed: 17880393]

Ricardo JA, Koh ET. Anatomical evidence of direct projections from the nucleus of the solitary tract to the hypothalamus, amygdala, and other forebrain structures in the rat. Brain Research. 1978; 153(1):1–26. [PubMed: 679038]

Rosas-Arellano MP, Solano-Flores LP, Ciriello J. Co-localization of estrogen and angiotensin receptors within subfornical organ neurons. Brain Research. 1999; 837(1–2):254–262. [PubMed: 10434010]

Sanchez F, de Gomez-Villalobos MJ, Juarez I, Quevedo L, Flores G. Dendritic morphology of neurons in medial prefrontal cortex, hippocampus, and nucleus accumbens in adult SH rats. Synapse. 2011; 65(3):198–206. [PubMed: 20665725]

Seltzer A, Pinto JE, Viglione PN, Correa FM, Libertun C, Tsutsumi K, Steele MK, Saavedra JM. Estrogens regulate angiotensin-converting enzyme and angiotensin receptors in female rat anterior pituitary. Neuroendocrinology. 1992; 55(4):460–467. [PubMed: 1314339]

Seltzer A, Tsutsumi K, Shigematsu K, Saavedra JM. Reproductive hormones modulate angiotensin II AT1 receptors in the dorsomedial arcuate nucleus of the female rat. Endocrinology. 1993; 133(2): 939–941. [PubMed: 8344227]

Shors TJ, Chua C, Falduto J. Sex differences and opposite effects of stress on dendritic spine density in the male versus female hippocampus. The Journal of Neuroscience: the official journal of the Society for Neuroscience. 2001; 21(16):6292–6297. [PubMed: 11487652]

Shughrue PJ, Merchenthaler I. Distribution of estrogen receptor beta immunoreactivity in the rat central nervous system. The Journal of Comparative Neurology. 2001; 436(1):64–81. [PubMed: 11413547]

Sriramula S, Cardinale JP, Lazartigues E, Francis J. ACE2 overexpression in the paraventricular nucleus attenuates angiotensin II-induced hypertension. Cardiovascular Research. 2011; 92(3): 401–408. [PubMed: 21952934]

Swanson LW, Kuypers HG. The paraventricular nucleus of the hypothalamus: cytoarchitectonic subdivisions and organization of projections to the pituitary, dorsal vagal complex, and spinal cord as demonstrated by retrograde fluorescence double-labeling methods. The Journal of Comparative Neurology. 1980; 194(3):555–570. [PubMed: 7451682]

Swanson LW, Sawchenko PE. Paraventricular nucleus: a site for the integration of neuroendocrine and autonomic mechanisms. Neuroendocrinology. 1980; 31(6):410–417. [PubMed: 6109264]

Tanaka J, Miyakubo H, Okumura T, Sakamaki K, Hayashi Y. Estrogen decreases the responsiveness of subfornical organ neurons projecting to the hypothalamic paraventricular nucleus to angiotensin II in female rats. Neuroscience Letters. 2001; 307(3):155–158. [PubMed: 11438387]

Tang FR, Tan CK, Ling EA. A comparative study by retrograde neuronal tracing and substance P immunohistochemistry of sympathetic preganglionic neurons in spontaneously hypertensive rats and Wistar-Kyoto rats. Journal of Anatomy. 1995; 186 (Pt 1):197–207. [PubMed: 7544334]

Turner, CD.; Bagnara, JT. General Endocrinology. Philadelphia: W. B. Saunders; 1971.

Veerasingham SJ, Raizada MK. Brain renin-angiotensin system dysfunction in hypertension: recent advances and perspectives. British Journal of Pharmacology. 2003; 139(2):191–202. [PubMed: 12770924]

Vega E, de Gomez-Villalobos MJ, Flores G. Alteration in dendritic morphology of pyramidal neurons from the prefrontal cortex of rats with renovascular hypertension. Brain Research. 2004; 1021(1): 112–118. [PubMed: 15328038]

Volkmann K, Chen YY, Harris MP, Wullimann MF, Koster RW. The zebrafish cerebellar upper rhombic lip generates tegmental hindbrain nuclei by long-distance migration in an evolutionary conserved manner. The Journal of Comparative Neurology. 2010; 518(14):2794–2817. [PubMed: 20506476]

Wang G, Anrather J, Glass MJ, Tarsitano MJ, Zhou P, Frys KA, Pickel VM, Iadecola C. Nox2, Ca2+, and protein kinase C play a role in angiotensin II-induced free radical production in nucleus tractus solitarius. Hypertension. 2006; 48(3):482–489. [PubMed: 16894058]

Wang G, Coleman CG, Chan J, Faraco G, Marques-Lopes J, Milner TA, Guruju MR, Anrather J, Davisson RL, Iadecola C, Pickel VM. Angiotensin II slow-pressor hypertension enhances NMDA currents and NOX2-dependent superoxide production in hypothalamic paraventricular neurons. American Journal of Physiology Regulatory, Integrative and Comparative Physiology. 2013; 304(12):R1096–1106.

Wang G, Milner TA, Speth RC, Gore AC, Wu D, Iadecola C, Pierce JP. Sex differences in angiotensin signaling in bulbospinal neurons in the rat rostral ventrolateral medulla. American Journal of Physiology Regulatory, Integrative and Comparative Physiology. 2008; 295(4):R1149–1157.

Wei SG, Yu Y, Zhang ZH, Felder RB. Angiotensin II upregulates hypothalamic AT1 receptor expression in rats via the mitogen-activated protein kinase pathway. American Journal of Physiology Heart and Circulatory Physiology. 2009; 296(5):H1425–1433. [PubMed: 19286949]

Wenthold RJ, Prybylowski K, Standley S, Sans N, Petralia RS. Trafficking of NMDA receptors. Annual Review of Pharmacology and Toxicology. 2003; 43:335–358.

Wiinberg N, Hoegholm A, Christensen HR, Bang LE, Mikkelsen KL, Nielsen PE, Svendsen TL, Kampmann JP, Madsen NH, Bentzon MW. 24-h ambulatory blood pressure in 352 normal Danish subjects, related to age and gender. American Journal of Hypertension. 1995; 8(10 Pt 1):978–986. [PubMed: 8845079]

Wright JW, Roberts KA, Stubley LA, Hanesworth JM, Harding JW. Hypothalamic angiotensin release in response to AII or glutamic acid stimulation of the SFO in rats. Brain Research Bulletin. 1993; 31(6):649–654. [PubMed: 8100178]

Xue B, Johnson AK, Hay M. Sex differences in angiotensin II- and aldosterone-induced hypertension: the central protective effects of estrogen. American Journal of Physiology Regulatory, Integrative and Comparative Physiology. 2013a; 305(5):R459–463.

Xue B, Pamidimukkala J, Hay M. Sex differences in the development of angiotensin II-induced hypertension in conscious mice. American Journal of Physiology Heart and Circulatory Physiology. 2005; 288(5):H2177–2184. [PubMed: 15626687]

Xue B, Pamidimukkala J, Lubahn DB, Hay M. Estrogen receptor-alpha mediates estrogen protection from angiotensin II-induced hypertension in conscious female mice. American Journal of Physiology Heart and Circulatory Physiology. 2007; 292(4):H1770–1776. [PubMed: 17142339]

Xue B, Singh M, Guo F, Hay M, Johnson AK. Protective actions of estrogen on angiotensin II-induced hypertension: role of central nitric oxide. American Journal of Physiology Heart and Circulatory Physiology. 2009; 297(5):H1638–1646. [PubMed: 19734362]

Xue B, Zhang Z, Beltz TG, Guo F, Hay M, Johnson AK. Estrogen regulation of the brain renin-angiotensin system in protection against angiotensin II-induced sensitization of hypertension. American Journal of Physiology Heart and Circulatory Physiology. 2014

Xue B, Zhang Z, Beltz TG, Johnson RF, Guo F, Hay M, Johnson AK. Estrogen receptor-beta in the paraventricular nucleus and rostroventrolateral medulla plays an essential protective role in aldosterone/salt-induced hypertension in female rats. Hypertension. 2013b; 61(6):1255–1262. [PubMed: 23608653]

Xue B, Zhao Y, Johnson AK, Hay M. Central estrogen inhibition of angiotensin II-induced hypertension in male mice and the role of reactive oxygen species. American Journal of Physiology Heart and Circulatory Physiology. 2008; 295(3):H1025–H1032. [PubMed: 18599599]

Ye ZY, Li L, Li DP, Pan HL. Casein kinase 2-mediated synaptic GluN2A up-regulation increases N-methyl-D-aspartate receptor activity and excitability of hypothalamic neurons in hypertension. The Journal of Biological Chemistry. 2012; 287(21):17438–17446. [PubMed: 22474321]

Zhao H, Joseph J, Fales HM, Sokoloski EA, Levine RL, Vasquez-Vivar J, Kalyanaraman B. Detection and characterization of the product of hydroethidine and intracellular superoxide by HPLC and limitations of fluorescence. Proceedings of the National Academy of Sciences of the United States of America. 2005; 102(16):5727–5732. [PubMed: 15824309]

Zhao H, Kalivendi S, Zhang H, Joseph J, Nithipatikom K, Vasquez-Vivar J, Kalyanaraman B. Superoxide reacts with hydroethidine but forms a fluorescent product that is distinctly different from ethidium: potential implications in intracellular fluorescence detection of superoxide. Free Radical Biology & Medicine. 2003; 34(11):1359–1368. [PubMed: 12757846]

Zhou Y, Dirksen WP, Chen Y, Morris M, Zweier JL, Periasamy M. A major role for AT1b receptor in mouse mesenteric resistance vessels and its distribution in heart and neuroendocrine tissues. Journal of Molecular and Cellular Cardiology. 2005; 38(4):693–696. [PubMed: 15808846]

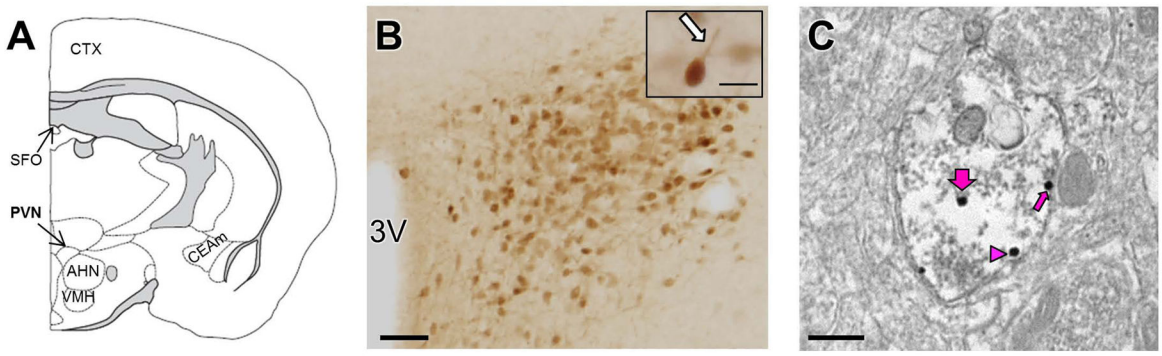

Figure 1. Angiotensin type 1A (AT1aR)-enhanced green fluorescent protein (EGFP)-labeled cells in the hypothalamic paraventricular nucleus (PVN)

A: Diagram of a coronal section of the mouse brain, showing a representative rostrocaudal level of the PVN containing AT1aR-EGFP [modified from Hof et al. (2000)]. B: Dense cluster of AT1aR-EGFP-containing cells in the PVN. Higher magnification (inset) shows that dendritic processes (arrow) of PVN neurons can be identified. C: Representative immunoelectron microscopic picture showing GluN1-silver-intensified immunogld (SIG) particles in an AT1aR-EGFP-labeled (immunoperoxidase) PVN dendrite. Immunoperoxidase labeling for AT1aR-EGFP (black arrow) was found throughout the cytoplasm of dendritic profiles. GluN1-SIG particles (black dots) were localized in the plasmalemma (thin magenta arrow), near the plasmalemma (magenta arrowhead), and in the cytoplasm (thick magenta arrow). 3V, third ventricle; AHN, anterior hypothalamic nucleus; CEAm, central nucleus of the amygdala, medial part; CTX, cortex; SFO, subfornical organ; VMH, ventromedial nucleus of the hypothalamus. Scale bars: B, C = 500 nm; Inset, 25 μm

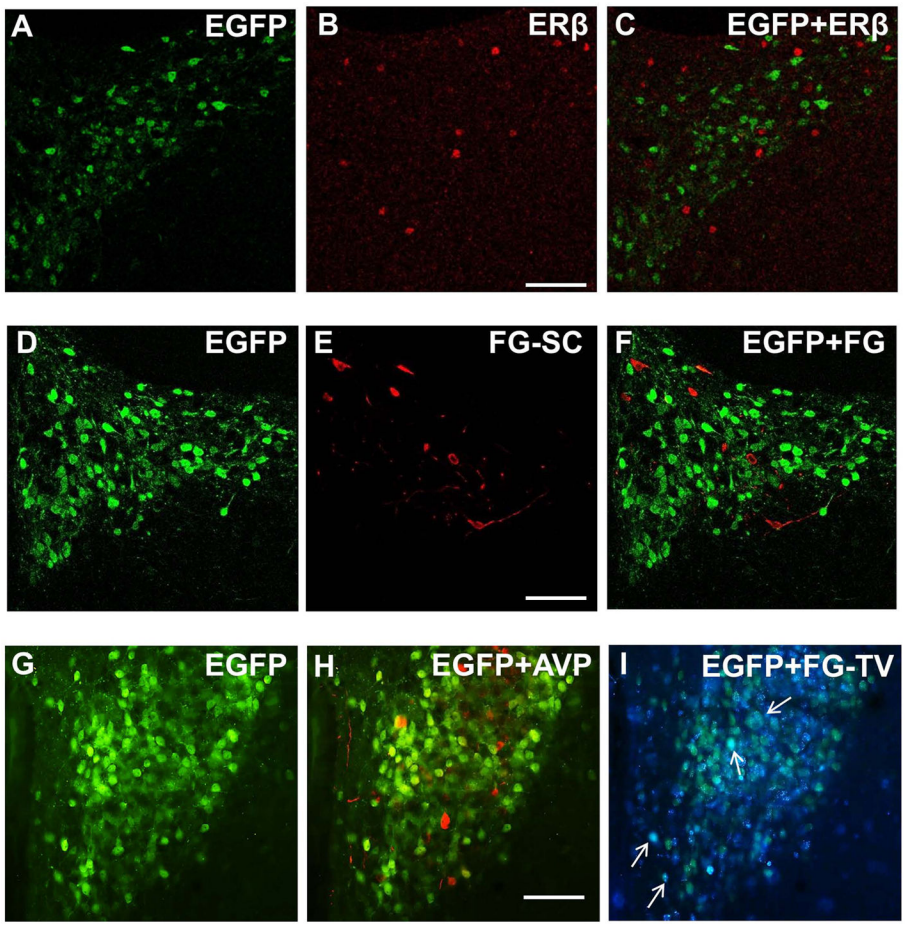

Figure 2. Distribution of AT1aR-EGFP-labeled cells in the PVN

A–C: AT1aR-EGFP and estrogen receptor β (ERβ) labeling of PVN neurons; A: AT1aR-EGFP PVN neurons (green) labeled with anti-GFP antiserum; B: PVN neurons labeled with anti-ERβ antiserum (red); C: merge of A and B showed no co-localization of GFP and ERβ. D–F: Spinally projecting PVN neurons; D: AT1aR-EGFP PVN neurons (green) labeled with anti-GFP antibody; E: PVN neurons labeled with fluorogold (FG, red) after injection into the spinal cord (FG-SC); F: Merge of D and E showed no co-localization of GFP and FG. G–I: AT1aR-EGFP, arginine-vasopressin (AVP) and tail vein-injected FG labeling of PVN neurons; G–I: PVN section triple labeled for GFP, AVP and FG following tail-vein (FG-TV) injection. G. AT1aR-EGFP PVN neurons (green) labeled with anti-GFP antiserum; H: No co-localization of GFP (green) and AVP (red) was observed; I: Scarce co-localization (white arrows) of GFP (green) and FG-TV (blue) was observed. Scale bars A–I = 0.5 mm.

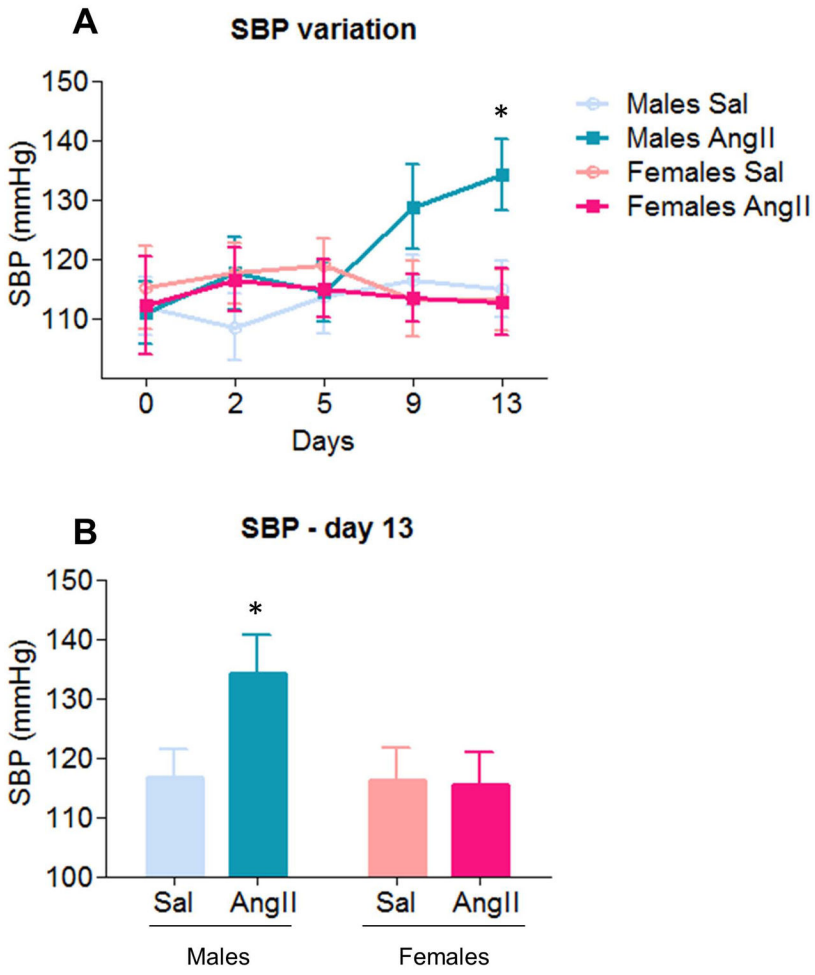

Figure 3. Angiotensin II (AngII) increases systolic blood pressure (SBP) in males but not in females

A–B: AngII infusion induced significant SBP increases ($p < .05$) in males on day 13. No additional differences were found in males or females. Sal, saline. *: $p < .05$

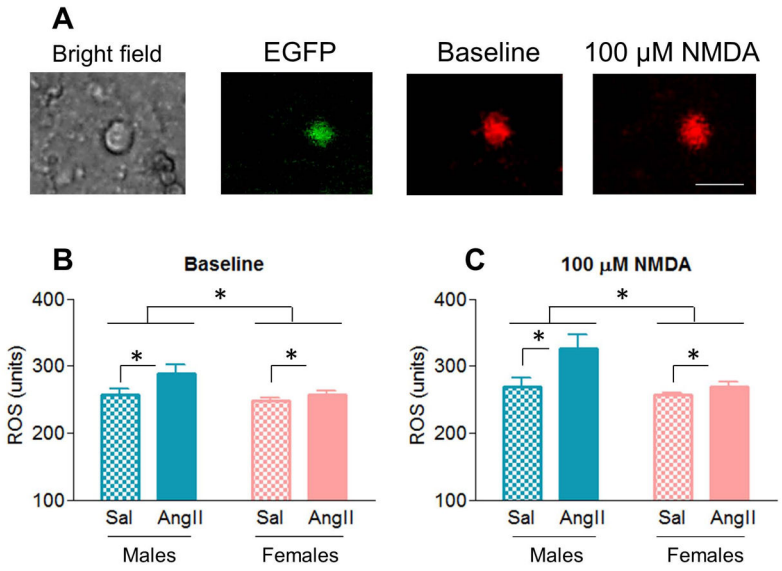

Figure 4. AngII increases ROS production in males but not in females

A: Representative images of AT1aR-EGFP PVN cells from an AngII-infused male mouse: bright field, EGFP (green) and ROS-dependent fluorescence (red) before and after the application of NMDA. B–C: ROS production was greater in AngII-infused animals than in saline controls ($p < .05$), in males than in females ($p < .05$), and post NMDA-administration than at baseline ($p < .001$). Scale bar = 20 µm. *: $p < .05$

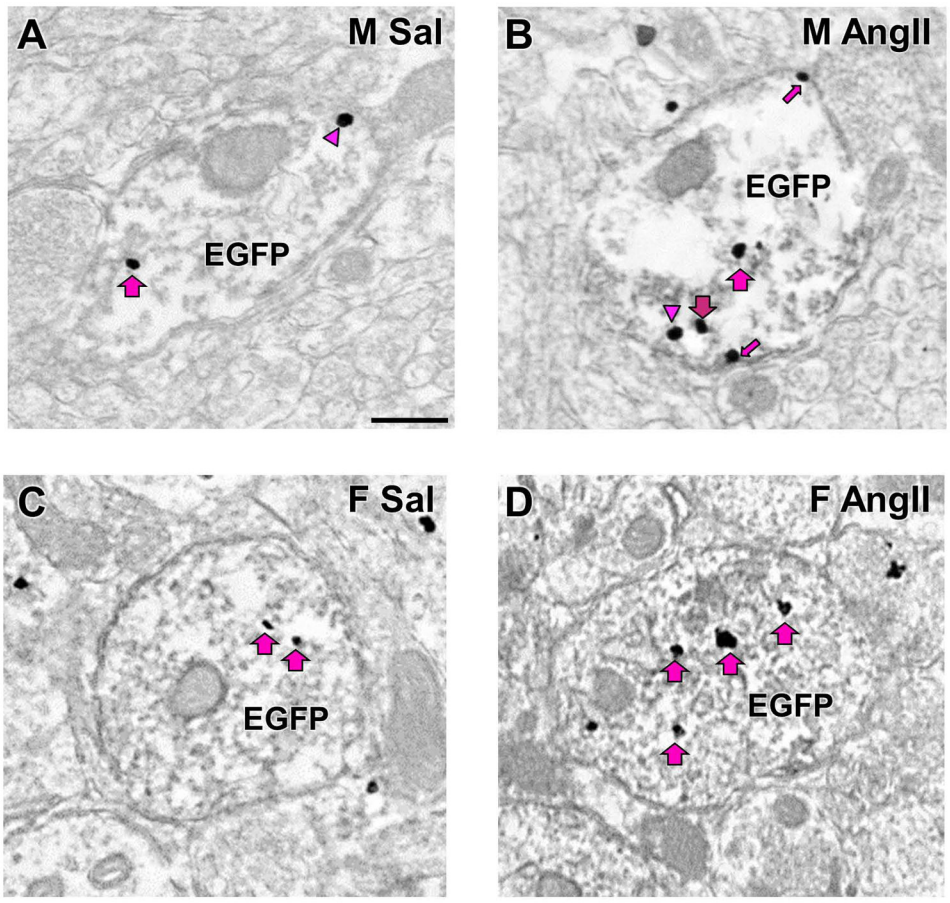

Figure 5. Representative electron micrographs of AT1aR-EGFP-containing dendrites

A: Males+saline; B: Males+AngII; C: Females+saline; D: Females+AngII. Examples of plasmalemmal (small arrow), near plasmalemmal (arrowhead) and cytoplasmic (large arrow) are shown. Scale bar = 500 nm

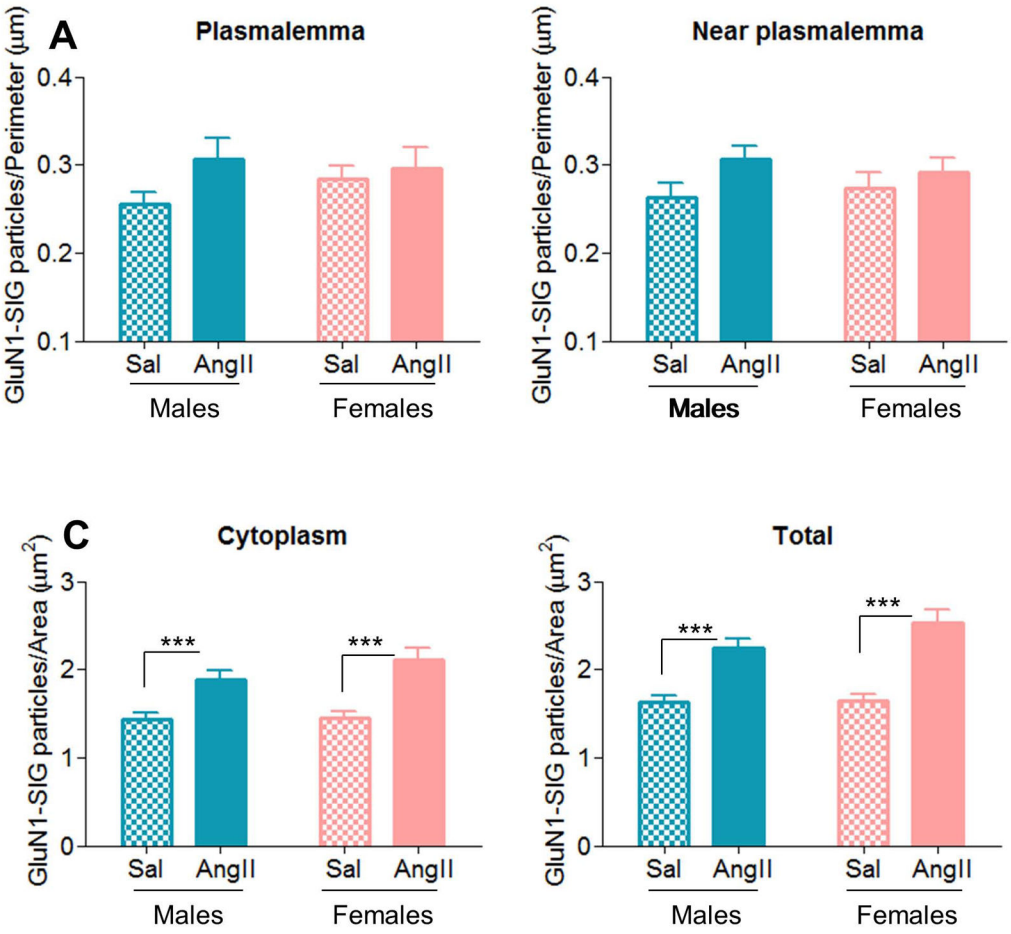

Figure 6. AngII infusion increases GluN1 density in AT1aR-EGFP-labeled PVN dendrites in males and females

A: In AT1aR-EGFP dendrites, no effects were found in plasmalemmal GluN1-SIG density. B: AngII infusion induced a trend ($p = .05$, B) towards greater near plasmalemmal GluN1-SIG density in comparison to saline controls. C–D: AngII infusion significantly increased cytoplasmic ($p < .001$, C) and total ($p < .001$, D) GluN1-SIG densities in males and female mice relative to saline controls. ***: $p < .001$

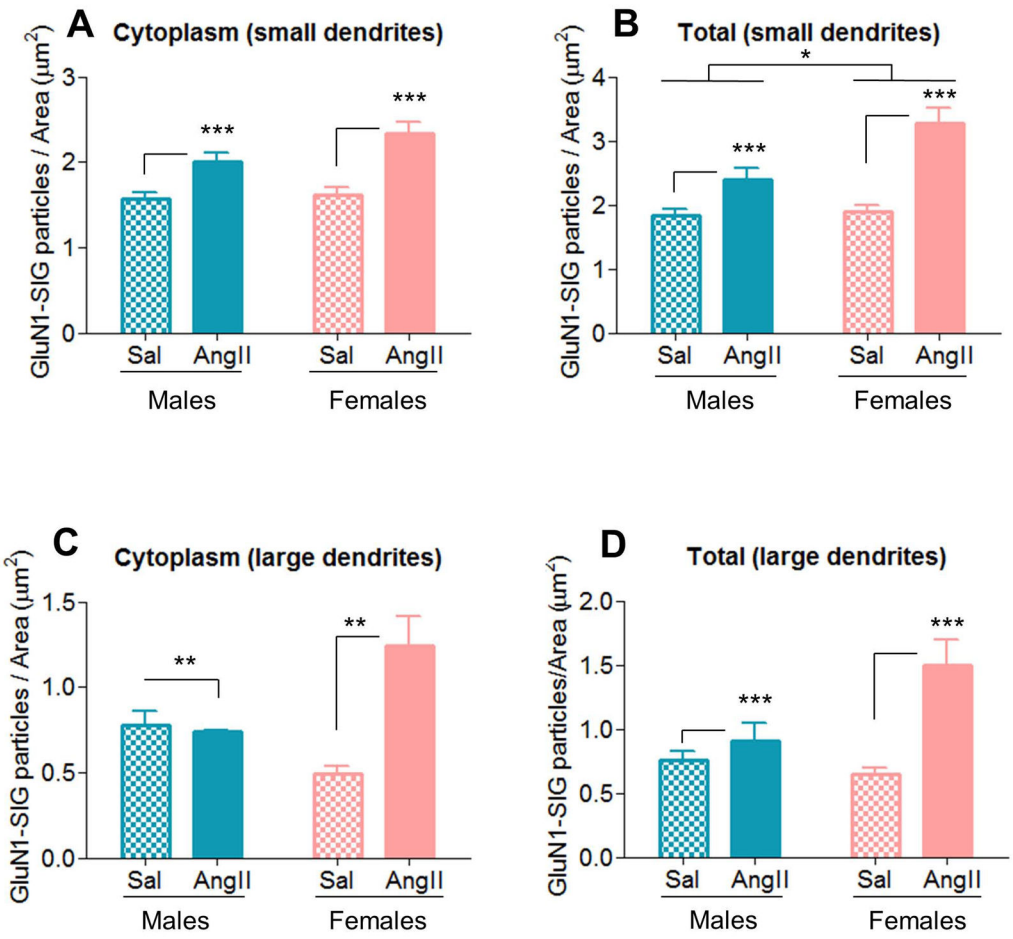

Figure 7. In AT1aR-EGFP-labeled PVN dendrites, AngII infusion increases GluN1 density similarly in males and females in small (distal) dendrites, but differentially in large (proximal) dendrites

A–B: In small AT1aR-EGFP dendrites, AngII infusion increased cytoplasmic ($p < .001$, A) and total ($p < .001$, B) GluN1-SIG density in males and female mice relative to saline controls. Moreover, a main effect of sex ($p < .05$) was also found in total GluN1SIG density (B). C–D: In large AT1aR-EGFP dendrites, differential changes in cytoplasmic (C) and total (D) to AngII infusion were observed in males and female mice. AngII infusion elicited opposite effects in cytoplasmicGluN1-SIG density in males (decrease) and females (increase) ($p < .01$, C), and increased total GluN1-SIG density in both males and females ($p < .001$, D). *: $p < .05$, **: $p < .01$, ***: $p < .001$

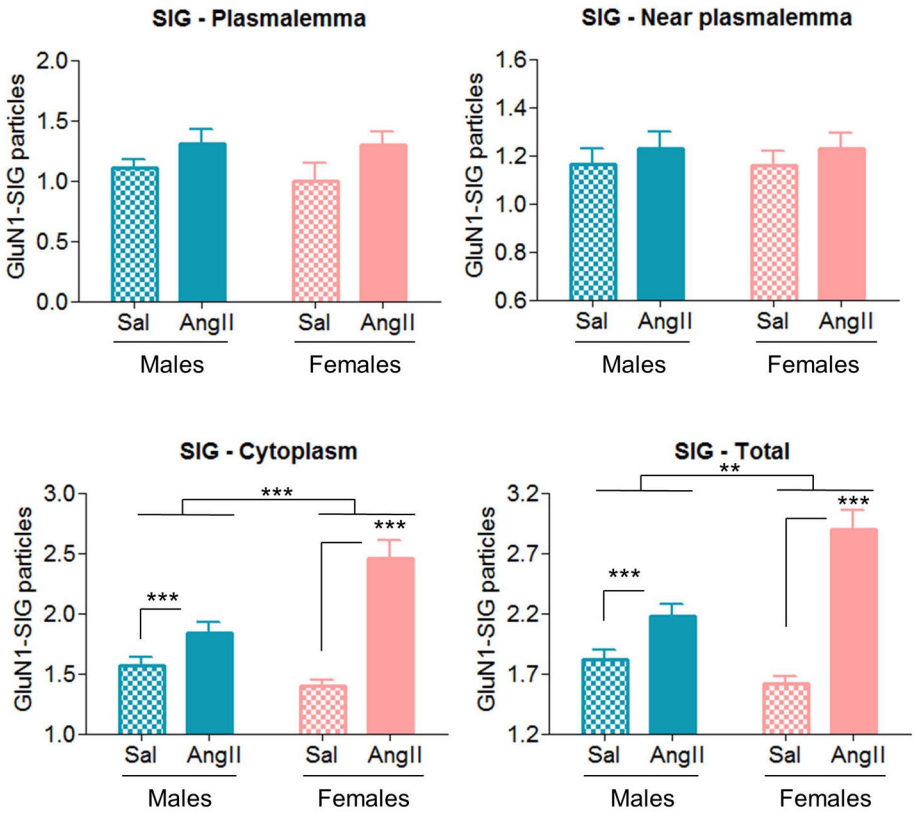

Figure 8. AngII infusion increases cytoplasmic and total GluN1-SIG counts in AT1aR-EGFP-labeled PVN dendrites in males and females

A–B: In AT1aR-EGFP dendrites, no differences were found in plasmalemmal (A) and near plasmalemmal (B) GluN1-SIG counts in males and females between AngII infusion and saline controls. C–D: AngII infusion significantly increased cytoplasmic ($p < .001$, C) and total ($p < .001$, D) GluN1-SIG densities in males and female mice relative to saline controls. Moreover, AngII infusion elicited a main effect of sex in cytoplasmic ($p < .001$) and total ($p < .01$) GluN1-SIG densities. **: $p < .01$, ***: $p < .001$

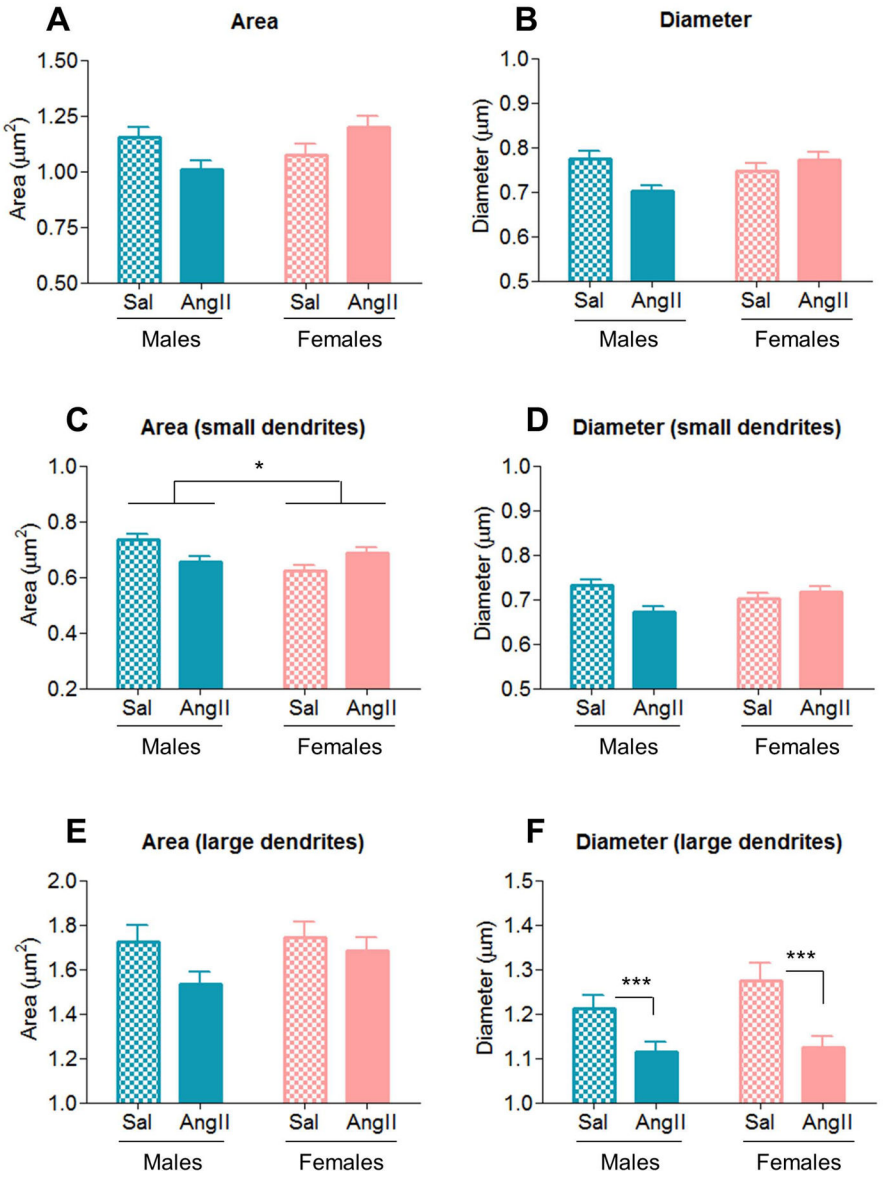

Figure 9. AngII infusion induces differential morphological changes in AT1aR-EGFP-containing PVN dendrites of males and female mice

A–D: AngII infusion elicited opposite effects in area and diameter of all (small and large) and of small AT1aR-EGFP-containing PVN dendrites of males (decrease) and females (increase), in comparison to saline controls. In addition, AngII infusion evoked main effect of sex in area of small dendrites. E–F: In large AT1aR-EGFP PVN dendrites, no effects were observed in dendritic area (E), but AngII significantly decreased ($p < .001$, D) dendritic diameter in both males and females. *: $p < .05$, ***: $p < .001$

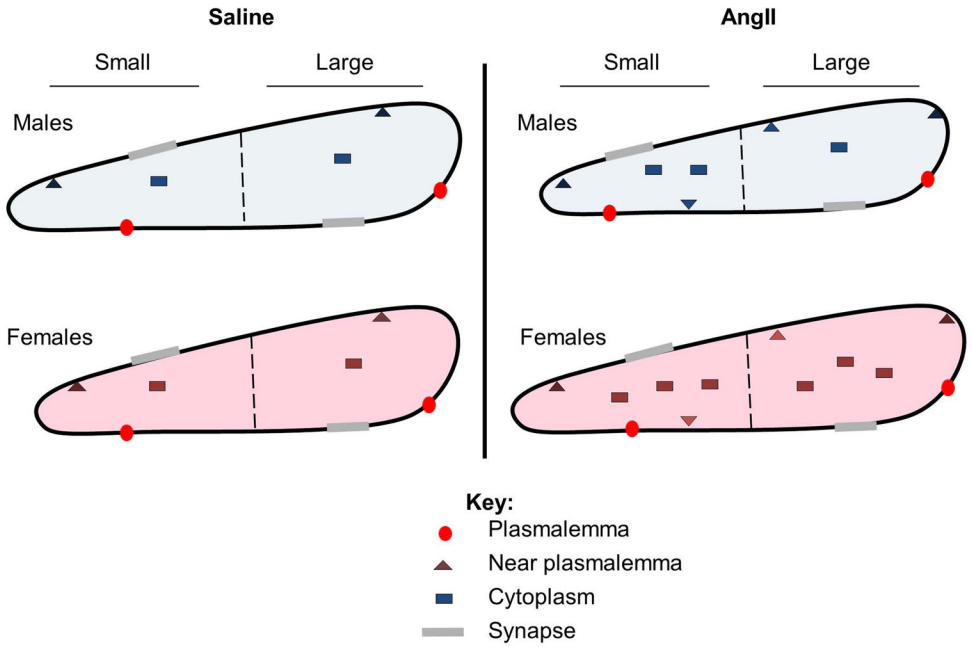

Figure 10. Schematic diagram summarizing AngII-induced effects in density and trafficking of GluN1 in AT1aR-EGFP dendrites in the PVN

GluN1-SIG particles are located on the plasmalemma (circle), near the plasmalemma (triangle) and in the cytoplasm (square) of AT1aR-EGFP dendrites. Dashed line indicates division between small and large AT1aR-EGFP dendrites and gray shadings on membranes indicate synapses. In males, AngII infusion increases cytoplasmic (small dendrites) and total GluN1-SIG density in AT1aR-EGFP dendrites in comparison with saline-infused controls. Moreover, AngII infusion decreases AT1aR-EGFP dendritic area and diameter in males. In females, AngII infusion increases cytoplasmic and total GluN1-SIG density in AT1aR-EGFP dendrites relative to saline-infused controls. In addition, AngII infusion increases area (small dendrites) and decreases diameter (large dendrites) of AT1aR-EGFP dendrites.